Summer 2015

Practical application of topology optimization to the design of large wind turbine towers

Brandon Lee Warshawsky
University of Iowa

PRACTICAL APPLICATION OF TOPOLOGY OPTIMIZATION TO THE DESIGN OF LARGE WIND TURBINE TOWERS

by

Brandon Lee Warshawsky

A thesis submitted in partial fulfillment
of the requirements for the
Master of Science degree in
Civil and Environmental Engineering
in the Graduate College of
The University of Iowa

August 2015

Thesis Supervisor: Professor Colby C. Swan

Graduate College
The University of Iowa
Iowa City, Iowa

CERTIFICATE OF APPROVAL

MASTER'S THESIS

This is to certify that the Master's thesis of

Brandon Lee Warshawsky

has been approved by the Examining Committee
for the thesis requirement for the Master of Science
degree in Civil and Environmental Engineering
at the August 2015 graduation.

Thesis Committee: _____
Colby C. Swan, Thesis Supervisor

_____
Jasbir S. Arora

_____
Salam Rahmatalla

ACKNOWLEDGMENTS

I would like to express my appreciation, for the support, guidance and advice that I have received from my parents, in my pursuit of my master's degree. I would not be here if not for your help.

Also I would like to thank my adviser, Professor Colby C. Swan, for his mentorship as well as all his help and advice throughout my time at the University of Iowa.

ABSTRACT

Structural topology optimization is a mathematical approach developed to perform design optimization with the purpose of reducing the material usage, while maximizing structural performance, in accordance to specific design constraints. The principles behind this technique have been around for many decades, but recent advancements in the processing power of computers have allowed for the solving of complex problems, such as the optimization of tall wind turbine towers, bridges, and the bracing systems in skyscrapers.

There are two approaches commonly used in structural topology optimization: discrete and continuum. This thesis uses continuum topology optimization, which involves adjusting the distribution of a porous elastic solid material to extremize the design objective(s) and to satisfy constraints. The material porosity is the design variable that is adjusted during the optimization process. The design domain is broken down into a system of continuum degenerated finite elements, which are used for both structural analysis and to create a mesh representation of the structural system, just as pixels make up a picture. Solid elements are modeled as having no porosity, while void spaces have total porosity. As the optimization process occurs, the shape of the boundaries, and the number and size of internal holes are altered in order to best meet the design objective(s) and constraint(s). The purpose of performing continuum structural topology optimization of structural elements is to obtain promising concepts which provide a basis upon which to begin the design process.

The steps taken in this thesis to optimize the wind turbine tower are:

1. Create a solid model of the tower domain

2. Define the material properties

3. Determine the equivalent static design wind forces using the extreme loading conditions outlined in IEC 61400

4. Formulate the optimization problem by specifying the objective and constraint functions.

5. Solve the optimization problem and interpret the results.

This study on continuum topology optimization on the tower shell, indicates even with a significant reduction in material from the original design space, the structure is capable of meeting the design criteria. The results indicate that opening void spaces in the shell of the tower and creating an open lattice shape may be an effective method to reduce the volume of wind turbine towers, as it has in other applications. This concurs with the stated goal of my research, which is to show that topology optimization has the potential to be used in a multitude of practical applications in order to increase efficiency, and reduce cost of the production of wind power.

PUBLIC ABSTRACT

Structural topology optimization is a mathematical approach, which can refine the physical layout of the material within a system to the optimal distribution based on a set of design criteria. The procedure has traditionally been used to achieve a reduction in mass of small manufactured parts, but can also be used to solve larger, more complex problems such as the design of bridges, skyscrapers, and wind turbine towers.

This thesis' study on the effectiveness of topology optimization on the tower of a wind turbine had two stated objectives: to explore the field of structural topology optimization and its potential uses, and to then use topology optimization to solve for the ideal open lattice shape for the turbine tower under specific loading conditions.

The results of this thesis indicate that significant reduction in material from the original design space is possible while still meeting the design criteria. The results indicate that by opening holes in the shell of the tower, to create a design similar to that of an open lattice structure, one can achieve a structure that efficiently uses the volume of material in wind turbine tower. This aligns with the purpose of my research, which is to show that topology optimization has the potential to be used in a multitude of practical applications to increase efficiency, and reduce cost of production of wind power.

TABLE OF CONTENTS

LIST OF TABLES

LIST OF FIGURES

CHAPTER 1. INTRODUCTION

1.1 Wind Turbine Background

With a growing global demand for energy coupled with the desire to transition away from a reliance on fossil fuels, the field of renewable energy production has a very large growth potential in the near future. Renewable energy is produced from resources that are replenished through natural processes over a short time period. This generally includes solar, wind, hydro-power, and photosynthetic energy. It has the potential to be the solution to many of the issues associated with the production of electricity using fossil fuels. There are two major problems associated with the production of energy from fossil fuels. The first is the release of greenhouse gases during production, and the other is the limited supply of accessible fossil fuels that remain.

Greenhouse gases are any gases that contribute to the greenhouse effect, which traps heat in the atmosphere. Energy production from fossil fuels release greenhouse gases into the atmosphere at a rate faster than can be naturally reabsorbed. The buildup in greenhouse gasses is believed to be the cause of an increase in the average global temperature, the melting of the polar ice caps, and an increase extreme weather.

In 2011, 21% of the global electricity market was produced from renewable sources, with an U.S. Energy Information Administration estimated projection of 25% by 2040 [66]. Electricity currently represents 39% of the total energy market; this percentage is expected to grow because of the introduction of electric vehicles and the dwindling supply of crude oil, which is expected to last only another 53 years [16].

Many governments around the world have implemented renewable energy goals including: the European Union, China, Japan, among others. While the United States has yet to set a goal or standard for the production of renewable energy, many states, including Iowa, Minnesota, Wisconsin and Illinois, have implemented their own.

The European Union aims to produce 20% of its energy from renewable resources by 2020 and increase that percentage to 27% by 2030 [45]. This incremental transition of energy sources is expected to cut greenhouse emissions by 40% compared to the 1990 levels. The European Union

currently has 14% of their power produced by renewables [45], which means that there are going to be a large number of energy infrastructure projects in the coming years to meet the goals set forth by the European Union Energy Counsel.

In the United States more than half of states have implemented renewable energy standards or goals. The policies range from a non-binding goal of 10% of power produced by renewable sources (North and South Dakota) to an enforceable standard of 33% by 2020 (California) [49]. The objective of these policies is to encourage the transition away from fossil fuels without raising electricity rates significantly, while encouraging the innovation and development of renewable technology.

The increased usage of renewable energy sources would reduce the reliance on foreign oil. It is estimated that the US being energy independent would have the potential to create hundreds of billions of dollars in economic stimulus and new jobs. It would also relieve some of the security concerns associated with the dependence on foreign oil.

In 2013, wind energy was the second fastest growing renewable energy sector, and fastest growing source of electricity in the United States, with more than 1100 Megawatts or 21% of new renewable energy created using wind as the primary source [58]. Wind is currently producing more than 5% of the total energy supply for the United States, and as shown in Table 1-1, is the fifth largest producer of energy.

Table 1-1: Total installed operating generating capacity in the United States: Through Dec. 2013

	Installed Capacity (GW)	% of Total Capacity
Coal	331.18	28.58%
Natural Gas	485.63	41.90%
Nuclear	107.32	9.26%
Oil	46.87	4.04%
Water	97.89	8.45%
Wind	60.60	5.23%
Biomass	15.80	1.36%
Geothermal Steam	3.84	0.33%
Solar	7.91	0.68%
Waste Heat	1.13	0.10%
Other	0.80	0.07%
Total	1,158.96	100.00%

Source: Data from Ventyx Global LLC

Figure 1-1 shows that there has been a dramatic increase in the number of wind turbines installed globally over the last twenty years. Wind power has shown an ability to produce clean electricity and that it can, and will play a crucial and substantial role in the transition from fossil fuels to renewable clean energy.

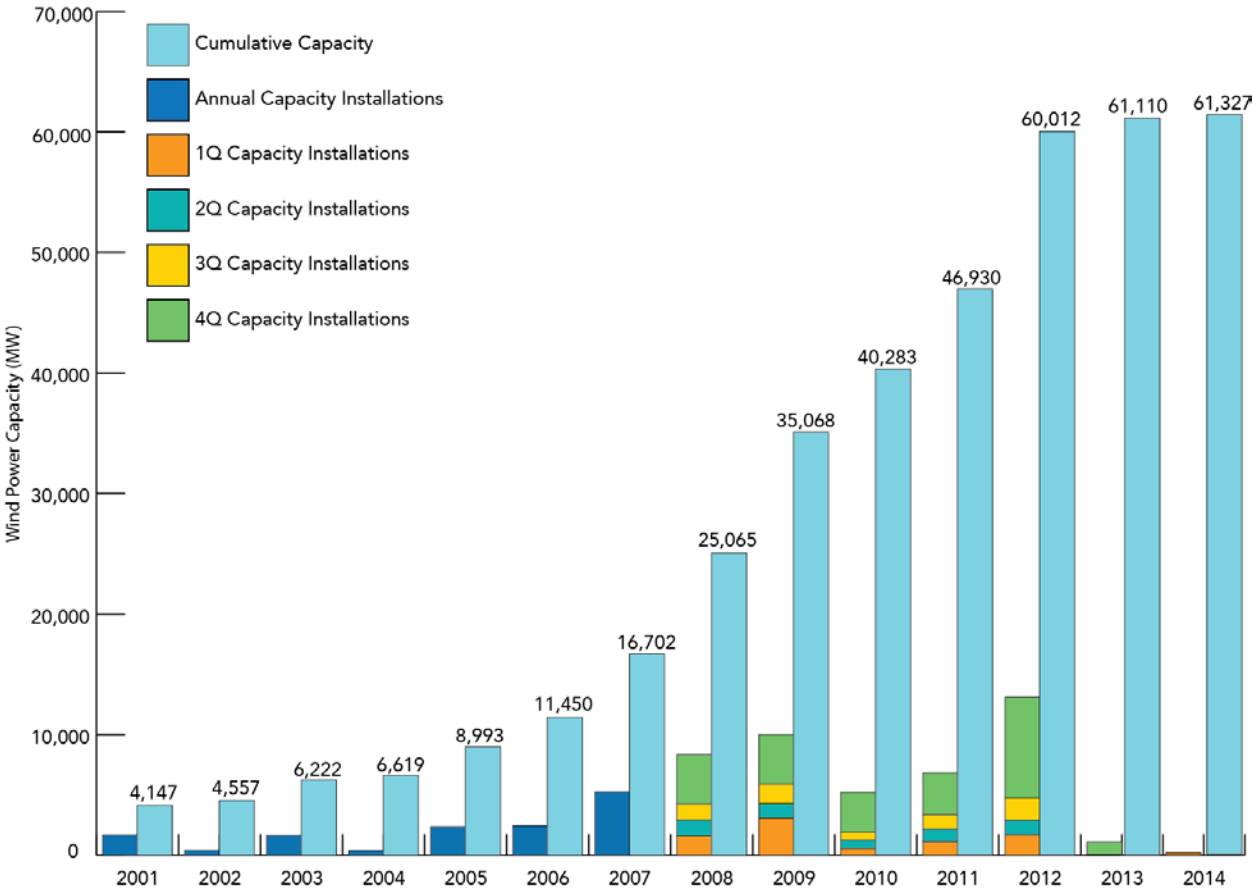

Figure 1-1: Total U.S. installed wind power capacity [69]

In the United States the average utility scale wind turbine operates at 1.3 MW. The latest generation of wind turbines are capable of operating at a capacity of 7.6 MW on just three times the amount of space; this results in a nearly 200% increase in the efficiency of energy production. To reach the higher capacity the wind turbine must have access to the large wind speeds, which occur at great heights. The greater speed enables the use of a higher resistance generator, which produces larger amounts of power. The 7.6 MW Enercon E-126 Wind Turbine uses a hub height of 135m and an overall height of 198.5m from base to blade tip to reach this increased capacity.

1.2 Why Optimize the Tower?

The capital cost is always a large factor in determining the relevance of an energy source in the renewable sector. With wind power, a large percentage of the price of the energy produced is due to the capital investment required to construct the wind turbine. In order for wind power to

become the choice in the transition from fossil fuels to renewable energy sources, the cost of the energy produced by wind power plants must rival the cost of energy produced by conventional coal. Wind power has an estimated levelized cost of approximately $85.60 per MWh, without subsidies; while coal produced electricity is currently at $60.00 per MWh [47]. Without a penalty for the production of greenhouse gasses, which would raise the price of energy produced by fossil fuels, the cost of renewable energy must come down to compete. Figure 1-2 shows the cost factors associated with the creation of wind power.

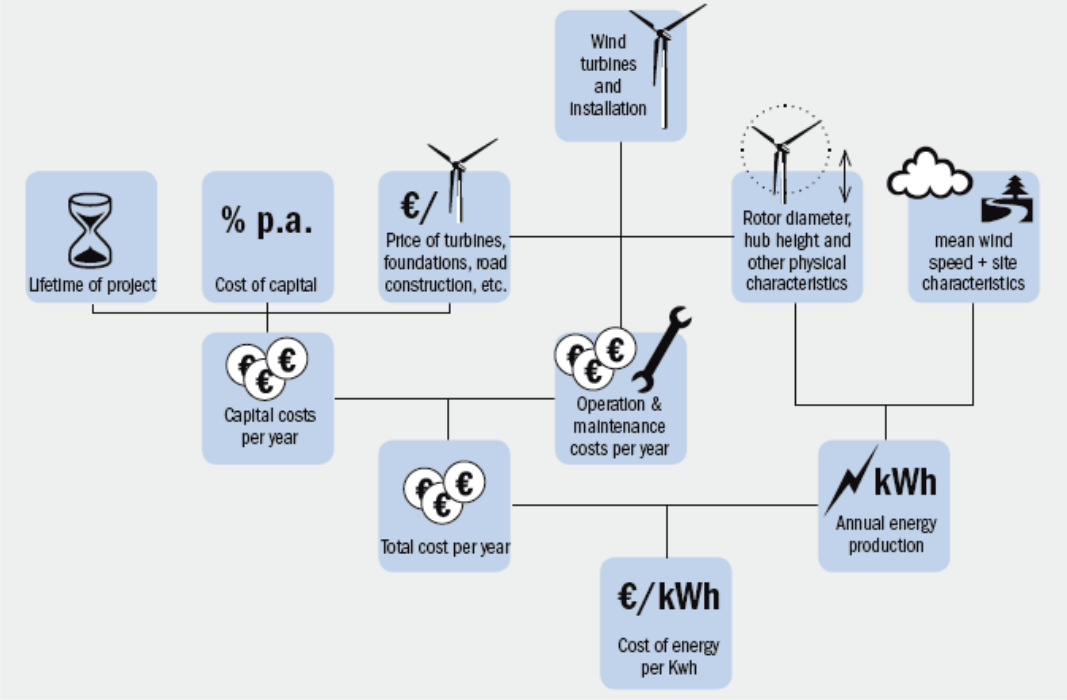

Figure 1-2: Costs that make up the price of energy created by wind power. [54]

There are two major ways to reduce the price of the electricity produced by wind energy; one is to improve the efficiency, and the other is to reduce the cost of the turbine. The tower of the average wind turbine is responsible for a large percentage of the total cost of production of wind turbines. For wind turbines with production for 5MW or more, which are referred to as "large commercial wind turbines," the tower typically makes up about a quarter of the capital cost of an average baseline turbine. The average relative cost for the wind turbine are shown in Figure 1-3. For the Enercon E-126 Wind Turbine the tower percentage represents $3.7 million of the $14 million total turbine cost.

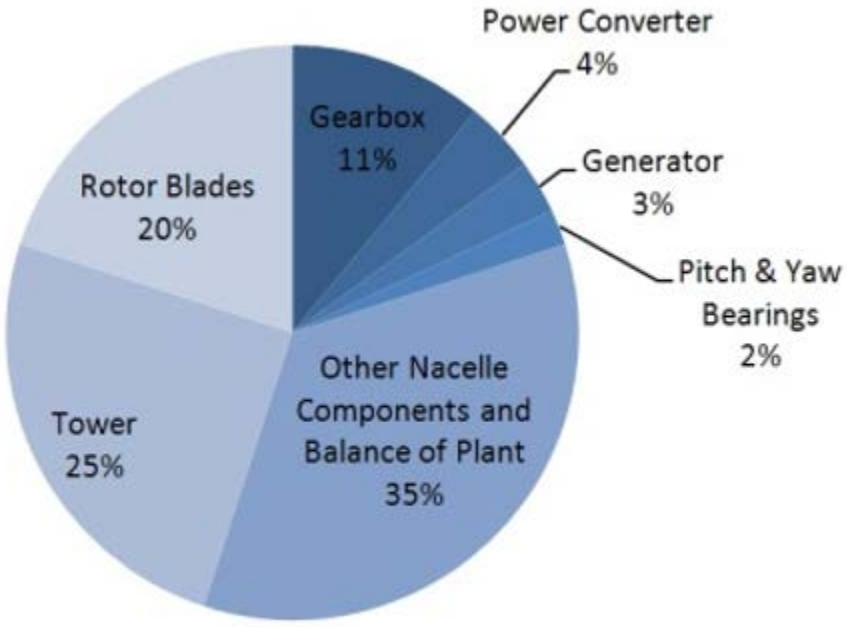

Figure 1-3: Cost breakdown for a wind turbine [73]

1.3 Objective

The primary objective of this research is to determine if topology optimization can be used to create an open lattice structure, which would reduce the volume of material that is used in the turbine tower in order to potentially reduce the capital cost. Open lattice structures are commonly used for small steel wind turbines with a hub height of up to 60m.

The goal of this thesis is to provide a baseline to determine if open lattice structures, which would be constructed using structural steel members can be used for the towers of the largest commercial wind turbines available today. It will also show how optimization techniques can be used in practical applications and potentially reduce cost of production.

1.4 Tower Being Optimized

To determine how effectively topology optimization can be used to transform the towers of the largest commercial wind turbines, a model of a tower similar to that of the Enercon E-126 7.6 MW wind turbine is created. The E-126 is currently the largest land based turbine in the world and can generate enough electricity for more than 5000 households. It is a logical choice to optimize because the towers are expected to get larger and larger in order to reach increasingly higher levels of efficiency. The full dimensional schematic of the turbine components for the E-126, have not been released to the public. Therefore interpolation between the known dimensions of the E-126 and those of the NREL 5-MW baseline wind turbine (which is the developmental turbine used in mid-size turbine analysis) is used to determine all the unknown dimensions.

1.5 Scope of Thesis

This thesis includes an introduction into the field of topology optimization, and its potential uses. Topology optimization is used to solve for the ideal open lattice shape for the turbine under extreme equivalent static wind loading with a 50-year recurrence period. The turbine blades are angled so that the largest drag forces that they can experience are achieved, and passed to the tower system. The forces from the rotation of the blades are not taken into account for this project due to the assumption that the lift forces mainly facilitate rotation and are negligible to the bending forces applied to the tower. The solution of the optimization program provides a starting point for the design process, and further work is required to create a design to be used in construction.

CHAPTER 2. COMPONENTS AND LOADS

2.1 Components of a Wind Turbine

The primary components of wind turbines (Figure 2-1) are the foundations, towers, nacelle, and rotor blades.

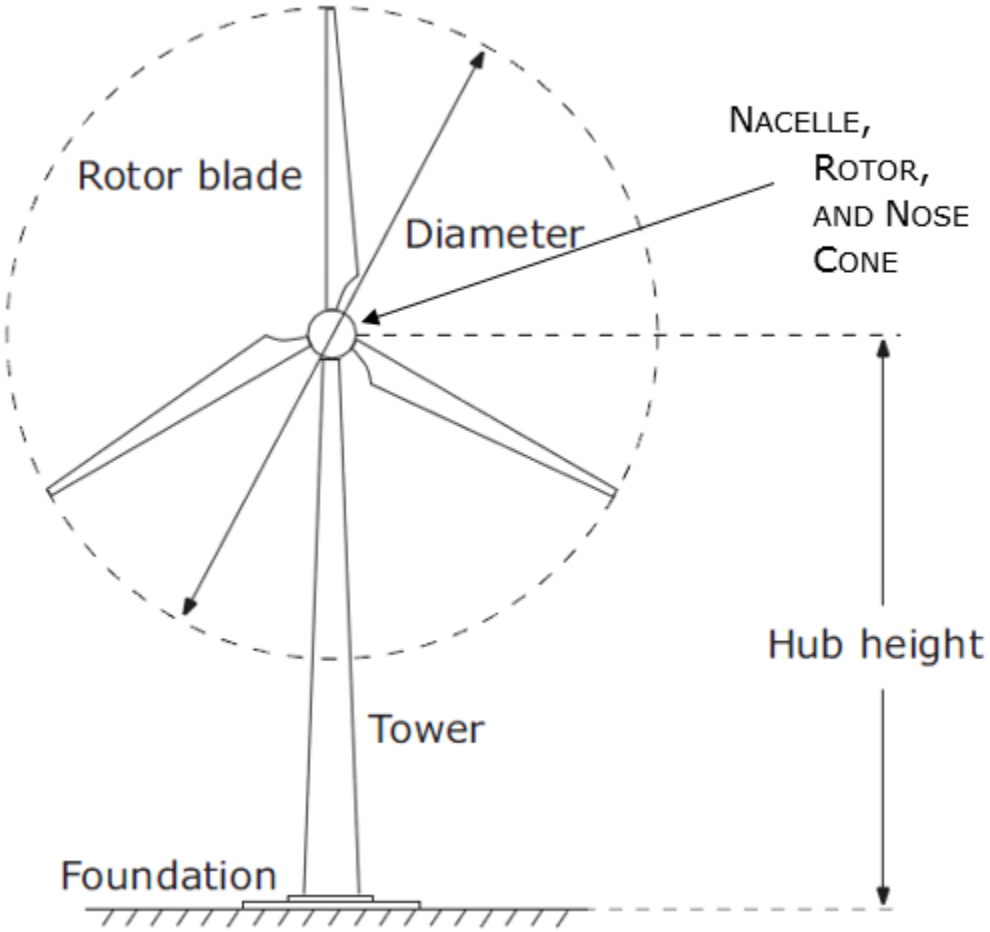

Figure 2-1: Wind turbine components

2.1.1 Foundation

The tower foundation ensures the stability of the wind turbine. Traditionally there are three types of foundations that can be used in wind turbine design: slab, soil stabilized, and pile. The type of foundation that is used for a tower is based on the soil conditions at the construction site.

Slab foundations, also known as mat foundation spread the load from the turbine onto a larger area, to prevent the tower from overturning. This type of foundation is best suited for stiff soils with a high friction angle. Equation Chapter (Next) Section 1

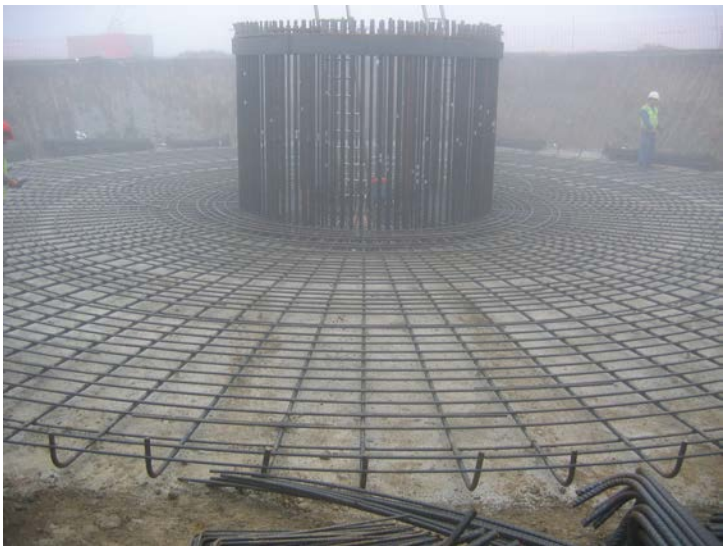

Figure 2-2: Rebar layout for slab foundation [17]

Soil-stabilized foundations manipulate the properties of the soil below the tower with chemical or mechanical treatments to improve its strength and stiffness. There are several different ways that the soil properties can be enhanced. The soil can be preloaded, compacted, or additional material can be added to reinforce the critical region. A common technique is jet grouting, a process which creates a column of soil-grout mixture to reinforce the soil. The process is used in poor quality soils where driving piles to bedrock is not feasible.

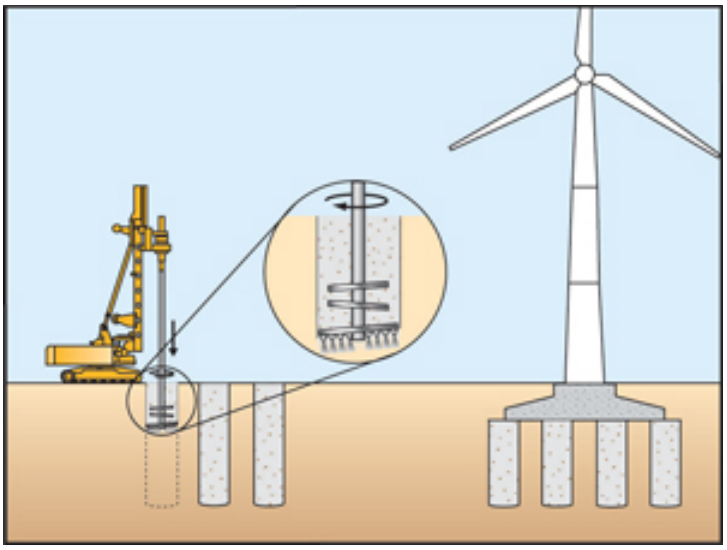

Figure 2-3: Soil stabilization process [10]

Pile foundations are used when the soil properties on the ground are not conducive to support a slab foundation. The piles conduct the load to better strength soil at a deeper depth, or bedrock, which provide the support needed for the tower. The piles employ tensile forces, to counteract the overturning moment caused by the wind forces on the tower. The tensile forces cause the connection between the pile and the tower to be a critical component.

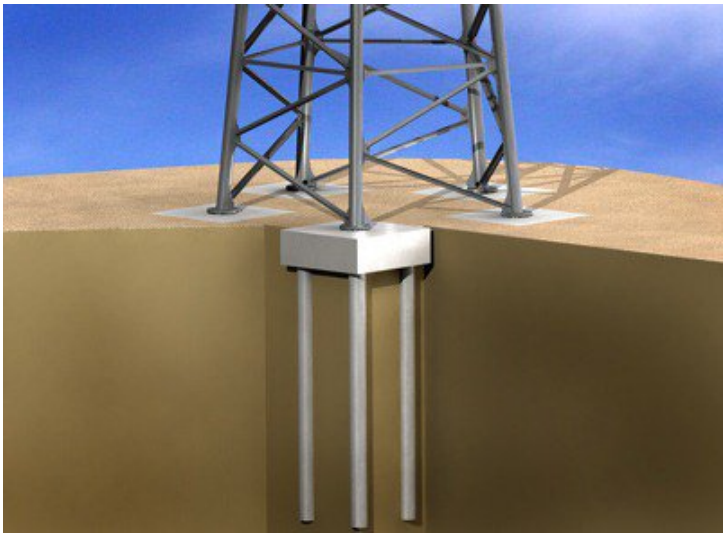

Figure 2-4: Pile foundation [43]

2.1.2 Tower

The tower is one of the most critical parts of the wind turbine structure. It is responsible for supporting the turbine and allowing it to reach the desired height. The higher the operating height of the wind turbine, the more electricity it can generate. The E-126 tower is fitted with an elevator with a capacity of 3-4 people which covers the span from the first floor to the top 15-20 meters of the tower, from there a spiral staircase, instead of the traditional ladders, connects the elevator to the nacelle.

There are three major types of towers: tubular steel, concrete, or steel lattice. They must be capable of supporting large gravity loads, as well as shear and bending moments created from the wind loading. The Enercon E-126 is constructed out of 35 precast concrete segments with walls that have a maximum thickness of 45 cm.

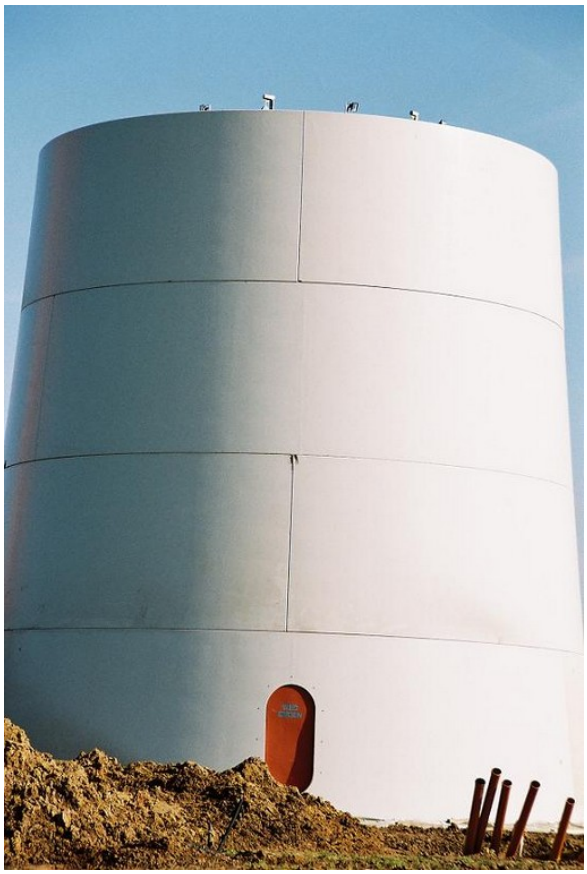

Figure 2-5: Enercon E-126 tower section [13]

The segments are transported to the site where they are installed and secured using steel prestressing tendons which run from the top of the tower through ducts located on the center-line of the wall and are anchored to the foundation, which is shown in Figure 2-6. The joints between the segments are filled using a high strength grout.

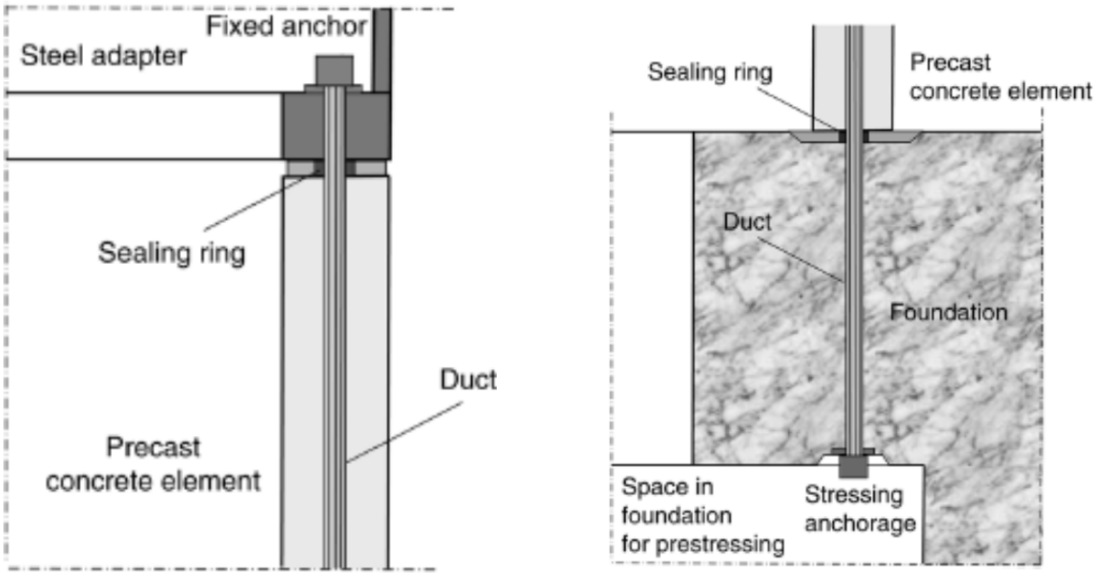

Figure 2-6: Anchor point for the prestressing cable to the top of the tower, and the foundation [20]

While the towers for large industrial wind turbines are traditionally constructed out of precast concrete segments, open lattice structures are usually constructed of steel members. The use of steel members allows for the mass production of the components, which has the ability to reduce the cost of production as well as the simplification of the construction process. For these reasons, this thesis uses the material properties of structural steel for the model.

2.1.3 Nacelle

The nacelle holds all of the critical machinery for the turbine. It contains the rotor shaft, transmission, coupling, a gearless generator, and brake. It is connected to the tower by bearings to allow for the nacelle to rotate with the direction of the wind. The generator of the Enercon E-126 is situated at the widest part of the nosecone and takes up the entire width of the nacelle, which enables it to produce power at the greatest efficiency. The turbine operates at 400V AC and is converted to DC current inside the nacelle.

Figure 2-7: Enercon E-126 nacelle [33]

2.1.4 Rotor Blade

The rotor and rotor blades use lift forces to convert the energy in the wind to rotate the rotor shaft. Utility size turbines use a three composite blade system. The blades have similar profiles to those of airplane wings to maximize the amount of lift, and efficiently rotate around the neutral axis. This varies from the mechanism used in traditional windmills, where the drag forces create rotation. The larger the area that is swept by the blades, the more power can be produced by the turbine. The Enercon E-126 has one of the largest swept areas of any land based wind turbine with a coverage of 12,668m^2.

Figure 2-8: Rotor hub and blades [37]

2.1.5 Hub

The hub is one of the heaviest parts of a wind turbine; it is usually made of cast iron, and connects the motor to the blades. The hub makes up a considerable portion of the mass of the rotor section. It uses a gear to move the motor, and create power. The hub is covered by the nose cone, which is aerodynamically designed to reduce some of the wind loading on the top of the system and protect the hub from the environment.

Figure 2-9: Enercon E-126 hub [44]

2.2 Tower Model Dimensions

The dimensions of the wind turbine model are similar to that of the Enercon E-126. The manufacturer provides limited dimensions, as shown in Table 2-1, therefore in order to determine the unknown taper of the tower, a photo of the turbine was scaled using AutoCAD 2015 and analyzed to determine the outer dimensions of the tower (Table 2-2). With very limited detail available on the thickness and material layout of the turbine tower, the tower is estimated to have a constant shell thickness of 20cm. The actual maximum thickness of the E-126 is 45 cm, however the volume of concrete used in the production of the tower, which is disclosed in the technical pamphlet, is much less than amount that would be expected with a

constant thickness. The inconsistency between the maximum thickness and the volume of concrete that is used in the production of the tower, allows for the assumption to be made that the reported maximum thickness is that of tower stiffeners and that the average thickness is much less.

Table 2-1: Known dimensions of the Enercon E-126

Known Characteristics of the Enercon E-126 wind turbine	
Base Diameter:	14.5 m
Top Diameter:	4.1 m
Hub Height:	135 m
Rotor diameter:	127 m
No. of blades:	3
Wind zone (DIBt):	WZ III
Wind class (IEC):	IEC/NVN IA

Table 2-2: Assumed dimensions of the Enercon E-126

Assumed Characteristics of the Enercon E-126 wind turbine	
Mid Point Diameter:	9.6 m
Mid Point Height:	38 m
Nacelle Height:	10.5 m
Nacelle Length:	14.3 m
Tower Thickness:	20 cm

2.3 Tower Loads

2.3.1 Input Parameters

Cross-sectional dimensions of the tower are inputs in the optimization process, shown in Figure 2-10.

d_{bo} = outer diameter of the tower base

d_{mo} = outer diameter of the tower at taper change

d_{to} = outer diameter of the tower top

t = thickness of the tower wall

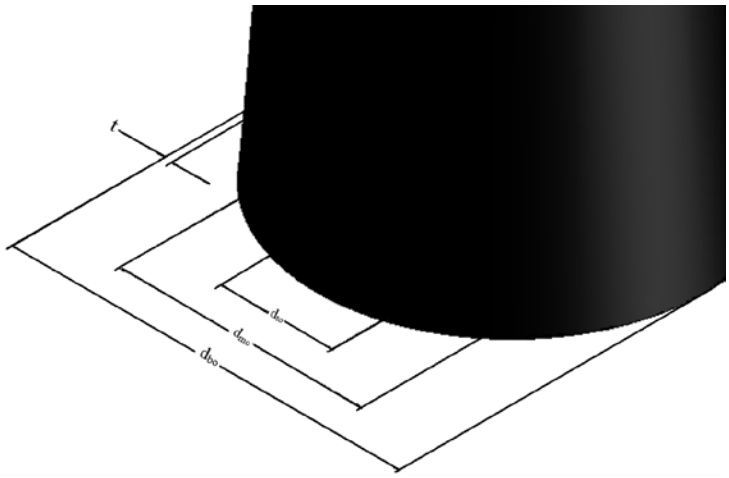

Figure 2-10: Cross sectional dimensions of the tower

Wind pressure calculation variables.

z_{hub} = the height of the center of the area swept by the turbine blades and rotor

V_{ref} = the basic parameter for wind speed that is used to define the wind turbine class.

V_{e50} = the expected extreme wind speed (average over 3 seconds), with a recurrence interval of 50 years

ρ = the density of air

C_p = the wind direction conversion factor

C_e = the exposure factor

C_q = the wind gust factor

I_w = the importance factor of the turbine

P_{en} = the effective force due to wind pressure on the nacelle

H = the height of the tower

E_s = the modulus of elasticity of steel

ρ_s = the density of steel

F_{RB} = the gravity load due to the rotor and blades

F_N = the gravity load due to the nacelle

α = the angle of attack of the turbine blade

C_D = the drag force coefficient of the turbine blade (function of the angle of attack)

C_F = the lift force coefficient of the turbine blade (function of the angle of attack)

D = the drag force experienced by the turbine blade

L = the lift force experienced by the turbine blade

c = the blade cord length

r = the radius of the turbine blade

Height Dependent Variables

q_s = the wind stagnation pressure

P = the wind stagnation force

P_e = the effective wind force

z = height

2.3.2 Structural Loading

The turbine components weights are provided by the manufacturer and are displayed in Table 2-3.

Table 2-3: Component masses

Mass of the Tower:	2800 ton
Mass of the Rotor:	264 ton
Mass of the Nacelle and Components:	348 ton
Mass of the Tubine Blade:	31 ton

The structural model of the wind turbine system, consists only of the tower itself, all exterior forces are applied in a consistent manner to the tower model. The gravity load of the tower is not taken into account in the model because the bending action cause by the loading is insignificant compared to the other loads acting on the tower. The tower is modeled without any added

structural support, such as an elevator shaft, in order to maximize the structural importance of the tower shell. The nacelle, rotor, and blades are not included in the model and therefore the resultant loads from the components are applied as nodal forces. The turbine is designed so that moment that is created due to the gravity loading of the turbine components, acts in the opposite direction of the bending caused by the wind load in an effort to limit the maximum deflection of the tower. The bending moments are created because the center of mass of the components does not fall on the neutral axis of the tower (refer to Figure 2-11).

Without a way to apply bending moments to the model in the finite element program, the moment was applied as a series of vertical forces which when combined act as the equivalent force and bending moment on the tower. The dimensions of the components are unknown; therefore the locations of their center of masses were interpolated from the NREL 5-MW baseline turbine to fit the dimensions of the E-126.

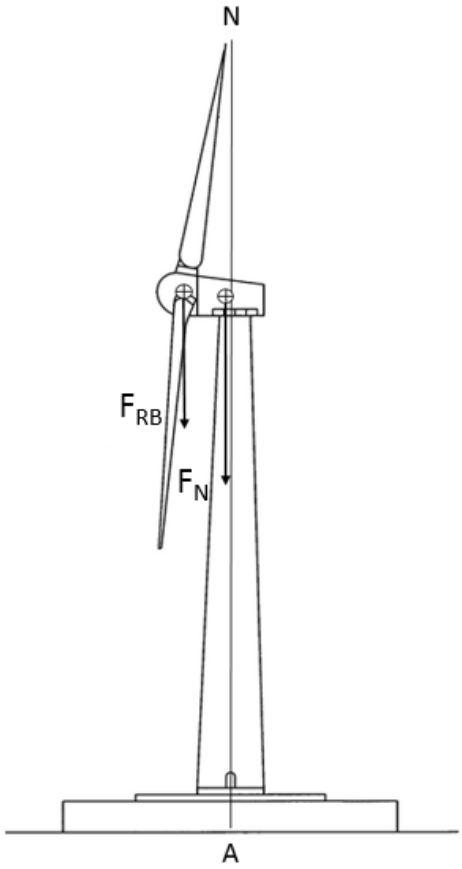

Figure 2-11: Diagram showing the location of the gravity loads of the rotor and blades and the nacelle (not to scale)

2.3.3 Wind Loading

The wind loading for the tower was determined for the extreme wind speed model, as defined in the International Standard for wind turbine design, published by the International Electrotechnical Commission. The wind loading is determined based on a number of criteria, representative of the environment that the turbine operates in.

The first criterion is the wind turbine class, which is defined based on the average reference velocity. The class is based on location of the tower, and symbolizes the average characteristics at the sites of installation, as shown in Table 2-4. The Enercon E-126 has a wind class of IA.

Table 2-4: Basic parameters for wind turbine classes [24]

Wind Turbine Class		I	II	III	S
V_{ref}	(m/s)	50	42.5	37.5	Values
A	I_{ref}	0.16			Specified
B	I_{ref}	0.14			by the
C	I_{ref}	0.12			Designer

The equation to determine the extreme wind speed that the tower experiences in a 50-year recurrence period is Eq. (2.1) [24]:

$$V_{e50}(z) = 1.4 \cdot V_{ref} \left(\frac{z}{z_{hub}}\right)^{0.11} \tag{2.1}$$

Where V_{ref} is the reference wind speed average over 10 minutes at hub height, and is found in Table 2-4, and z_{hub} of the tower is 135m. I_{ref} is the expected value of the turbulence intensity at 15m/s, this value is not used in the calculations. The wind loads are determined as stall pressures using Eq. (2.2), and are a function of the element surface area and the element height. [41]

$$P(z) = C_e \cdot C_q \cdot q_s \cdot I_w \tag{2.2}$$

This equation determines the design wind pressure using the wind stagnation pressure and coefficients based on the exposure, gust factors, shape and importance of the structure. The Uniform Building Code Volume 2, found in Table A-2 in the appendix, provides tables for the determination of the design pressure.

The stagnation pressure is found using the equation [24]:

$$q_s = \frac{1}{2}\rho \cdot V_{e50}(z)^2 \tag{2.3}$$

The coefficient of exposure is found using the equation [41]:

$$C_e = 0.5824z^{0.22} \tag{2.4}$$

The importance factor (I_w) for a wind turbine is a standard with the value [24]:

$$I_w = 1.15 \tag{2.5}$$

C_q is a pressure coefficient that is dependent on the shape of the face that the load is acting on. The coefficient is from the Uniform Building Code, and is listed for a 10 square-foot (0.93 m^2) tributary area. A higher value is provided for open frame towers, which accounts for the reduction in surface area resulting in a lower loading. Since the loading on the tower is not changed during the optimization process, the calculation for the wind loading on the tower uses the lower coefficient that used for solid structures [41].

$$C_q = 0.8 \tag{2.6}$$

The pressure at the stall point, the location where the wind direction is perpendicular to the face of the tower, is the effective load that would be experienced by the tower at each height increment. In order to design a tower model in which void space can be created without limitations on where these voids can occur, the total wind loading is applied as an equivalent horizontal load and bending moment, to the nodes located at the top of the tower. The bending moment that is applied to the tower allows for the loading that is experienced on the tower, to be applied to the nodes at the top of the tower, and be in static equilibrium.

2.3.3.1 Blade and Nacelle Wind Loading

The wind loading on the nacelle and nose cone is determined by modeling the nose cone as a round hemispherical cone. The pressure is that is experienced by the nacelle is found to be one half of that which would be experienced by a sphere of the same dimensions. [37] The pressure

that is experienced by the nose cone and nacelle can be described using Eq. (2.7), where A is the cross-sectional area of the nose cone. [37]

$$P_{en} = \frac{1}{2} q_s \cdot A \cdot C_e \cdot C_q \cdot I_w \tag{2.7}$$

The blades of the turbine are scaled from those used in the NREL 5-MW to fit the dimensions of the E-126. The forces acting on the blades are resolved into drag and lift forces using Eq. (2.8) and (2.9). These forces are maximized for the angle of attack, (α), to determine the maximum force the tower experiences due to the blade loadings.

The lift equation is represented as:

$$L = \int \frac{1}{2} \rho \cdot V_{e50}^2 \cdot c \cdot C_L \partial r \tag{2.8}$$

The drag equation is represented as:

$$D = \int \frac{1}{2} \rho \cdot V_{e50}^2 \cdot c \cdot C_D \partial r \tag{2.9}$$

The chord length is used as the width of the turbine blade; this chord length was scaled from the baseline turbine to better represent the longer blades of the E-126. The twist is the angle that the leading edge of the blade makes relative to the tip of the blade. These values are a property of the blade, and are not changed to maximize the drag force.

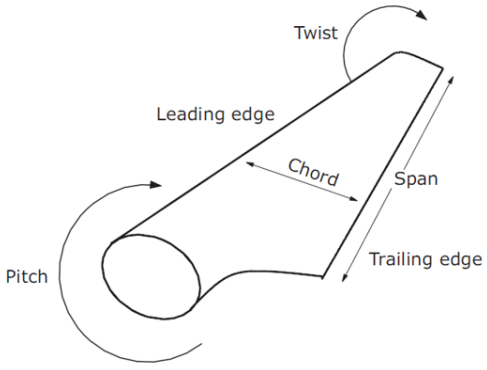

Figure 2-12: Turbine blade terminology

The angle of attack (α) is the angle that the chord line makes relative to the wind direction. A high angle of attack creates large drag forces. The loading that is applied to the model from the blades is the highest sum of the elemental forces. The elemental forces are determined by finding the angle of attack that creates the drag confidents for each section that result in the largest net drag force on the blade.

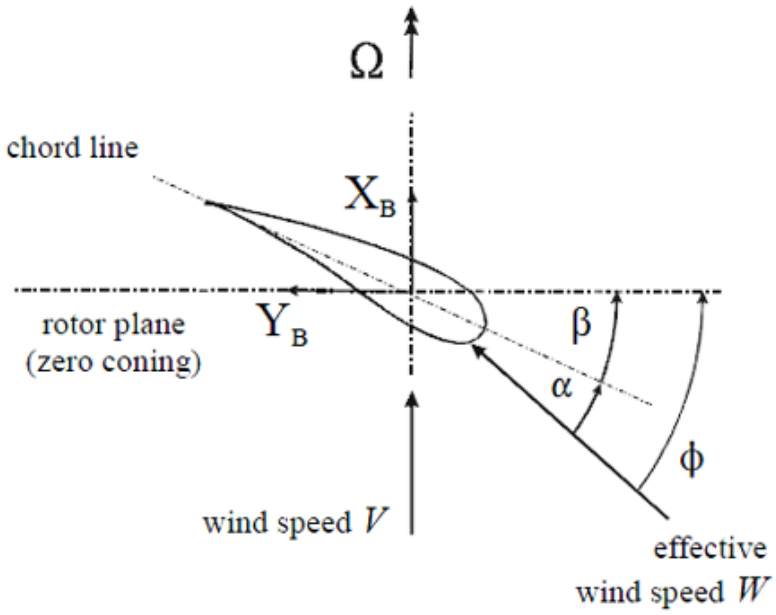

Figure 2-13: Angle of attack (α) [53]

The span of the turbine blades are broken up into a number of elements, each element has a constant length, and uses the airfoil information that best represents the blade at that section. The nodes start at the connection of the blades to the nose cone, the first node occurs at the radial length (Rnodes) of 2.95m from the centroid of the three blades. The airfoil tables are published by the National Advisory Committee for Aeronautics and provide information on the relationship between the angle of attack and the drag coefficient (C_D). [26]

The pitch of the blades was set to maximize the total drag force experienced by the blades. The blades were broken down into elements and the drag forces were determined for each segment. Only the drag forces which act in the horizontal direction are accounted for in the loading that is applied to the top of the tower, because the lift force mainly facilitates rotation of the rotor about a central axis.

Table 2-5: Drag force acting on a blade

Scaled E-126 Theoretical Turbine							
Node	Rnodes (m)	Twist (°)	Chord Length (m)	Airfoil Table	Angle of attack (°)	C_D	Drag Force (kN)
1	2.95	13.31	3.65	Cylinder1.dat	76.69	0.50	9.05
2	5.77	13.31	3.97	Cylinder1.dat	76.69	0.50	9.85
3	8.59	13.31	4.29	Cylinder2.dat	76.69	0.35	9.31
4	12.11	13.31	4.70	DU40_A17.dat	76.69	1.76	61.35
5	16.33	11.48	4.79	DU35_A17.dat	78.52	1.54	54.99
6	20.55	10.16	4.59	DU35_A17.dat	79.84	1.54	52.69
7	24.78	9.01	4.38	DU30_A17.dat	80.99	1.45	47.36
8	29.00	7.80	4.13	DU25_A17.dat	82.21	1.41	43.19
9	33.23	6.54	3.86	DU25_A17.dat	83.46	1.40	40.33
10	37.45	5.36	3.61	DU21_A17.dat	84.64	1.44	38.71
11	41.68	4.19	3.35	DU21_A17.dat	85.81	1.44	35.99
12	45.90	3.13	3.10	NACA64_A17.dat	86.88	1.43	33.00
13	50.12	2.32	2.85	NACA64_A17.dat	87.68	1.43	30.30
14	54.35	1.53	2.49	NACA64_A17.dat	88.47	1.46	22.49
15	57.87	0.86	2.38	NACA64_A17.dat	89.14	1.46	17.21
16	60.68	0.37	2.15	NACA64_A17.dat	89.63	1.46	15.52
17	63.50	0.11	1.46	NACA64_A17.dat	89.89	1.46	0
			Total Drag Force on Each Blade (kN)				521.34

The wind load that acts on the blades and the nose cone, as well as the gravity loading from the components which make up the turbine, are applied as vector forces to the nodes that comprise the top ring of the tower, and simulate the connection between the nacelle and the top section of the tower.

2.3.4 Tower Wind Loading

One of the limitations of the topology optimization software is that the loading is not linked to the porosity of the structure at the node where the load is being applied. A real world turbine tower would experience some wind load at every point of the tower. The loading that each node

would experience can be determined by modeling the exterior tower load as a fluid with the physical properties of air flowing past the cylindrical tower.

The wind pressures can be determined based on turbulent flow around the boundary layer of the cylinder. Experimental results for high Reynolds number flow over a circular cylinders, [8] can be fit by a high order polynomial equation to determine the effective loading that the tower experiences at different angles from the wind direction. Using the polynomial function to determine the effective pressure coefficient, the stall pressure coefficient equation displayed in Eq. (2.10), can be used transform the nodal stall pressure into the effective nodal pressure at any point of the tower.

The effective pressure coefficient (C_p) can be represented by the polynomial, where θ represents the angle from the stall point in degrees:

$$C_p = 0.142\cdot\theta^{10} - 2.327\cdot\theta^{9} + 15.923\cdot\theta^{8} - 59.087\cdot\theta^{7} + 129.192\cdot\theta^{6} - 169.808\cdot\theta^{5} + 131.252\cdot\theta^{4} - 53.454\cdot\theta^{3} + 6.315\cdot\theta^{2} - 0.758\cdot\theta + 1.002 \quad (2.10)$$

When plotted against the angle from the wind stall point, the pressure coefficient varies as shown in Figure 2-14.

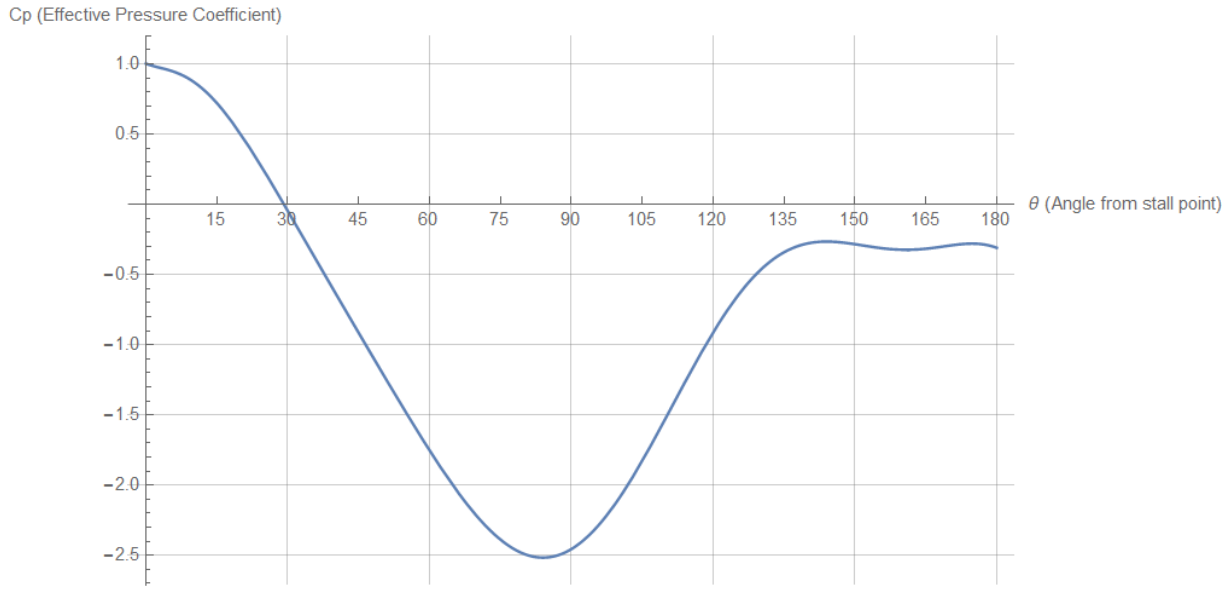

Figure 2-14: The plot of the effective pressure coefficient vs. the angle of the element from the stall point

This modeling technique enables the creation of load data for every node, which results in there being no points capable of being optimized to a “void” space, because the node would undergo massive deformation. To avoid this result and create a model where optimization would result in a reduction in the volume of structural material, all the loads are applied to the nodes that make up the top layer of the tower, using the procedure in chapter 2.5. The loads that are applied at these nodes are the combination of the gravity and wind load being transferred to the tower from the nacelle and blades, and the equivalent wind load and counteracting moment from the tower.

2.4 Gravity Load

The gravity loading on the tower is applied as nodal forces on the top ring of the tower. The forces were determined as an equivalent point load and bending moment (Figures 2-15 and 2-16).

Figure 2-15: Diagram showing the gravity load from the rotor and blades (not to scale)

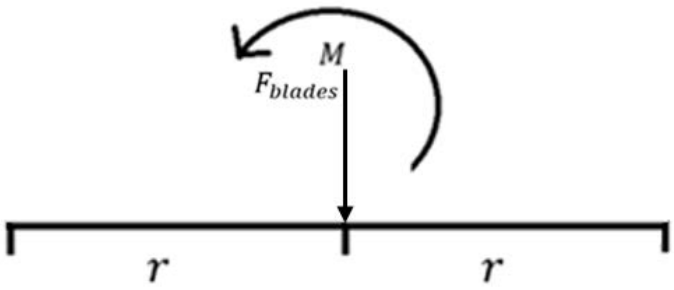

Figure 2-16: Diagram showing the equivalent point load and bending moment

The distributed load is transformed into equivalent point loads located at 2/3rds the span of the load (Figure 2-17). The gravity load has an eccentricity of 10 meters from the centroid of the tower into the wind.

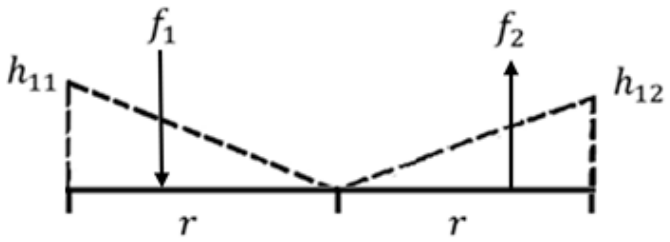

Figure 2-17: Diagram showing distributed loading represented by point loads located at 2/3rds the radius from the tower center (not to scale)

The sum of the two point loads are equivalent to that of the gravity load that the tower experiences due to the blades and rotor.

$$F_{blades} = f_1 - f_2 \tag{2.11}$$

Each point load represents the total area of the distributed load from the location of the outermost node to the centroid.

$$f_1 = \frac{1}{2} \cdot r \cdot h_{11} \tag{2.12}$$

$$f_2 = \frac{1}{2} \cdot r \cdot h_{12} \tag{2.13}$$

Setting the sum of the forces and moments equal to zero, a system of equations consisting of two equations and two unknowns can be set up to determine the relevant information about the created distributed loads.

$$F_{blades} \cdot x_c = f_1 \cdot \frac{2r}{3} + f_2 \cdot \frac{2r}{3} \tag{2.14}$$

The same procedure is used to create a distributed load to represent the force and bending moment that is caused by the mass of the nacelle. The distributed loads and equivalent point loading are shown in Figures 2-17, and 2-18 respectively.

Figure 2-18: Diagram showing the gravity load from the nacelle (not to scale)

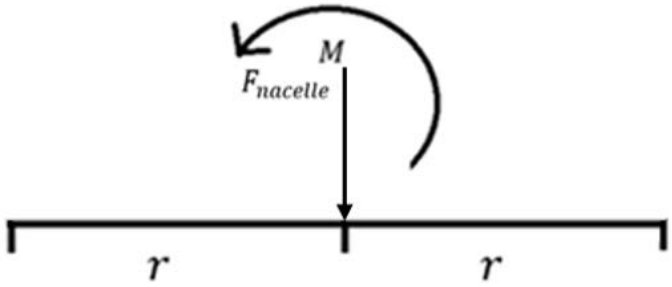

Figure 2-19: Diagram showing the equivalent point load and bending moment

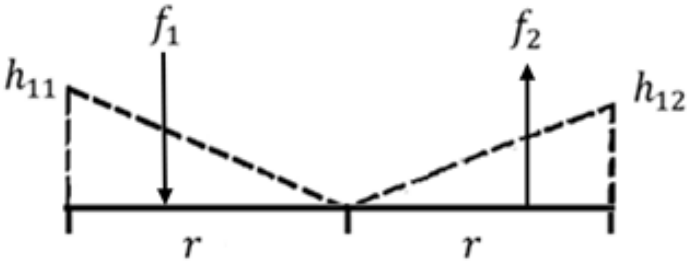

Figure 2-20: Diagram showing distributed loading represented by point loads located at 2/3rds the radius from the tower center (not to scale)

The diagrams are represented mathematically by the formulas below.

$$F_{nacelle} = f_1 - f_2 \tag{2.15}$$

$$f_1 = \frac{1}{2} \cdot r \cdot h_{21} \tag{2.16}$$

$$f_2 = \frac{1}{2} \cdot r \cdot h_{22} \tag{2.17}$$

$$F_{nacelle} \cdot x_c = f_1 \cdot \frac{2r}{3} + f_2 \cdot \frac{2r}{3} \tag{2.18}$$

Each node located on the top layer of the tower has the combined loading of these two forces applied as a vertical vector load. Triangular loads with the maximum loads determined from Eq.

(2.19) and (2.20) represent the combined distributed loading. The loadings are their maximum at the outer nodes that fall in the direction of the wind plane and slope to zero at the centroid. A plot showing the nodal gravity loads applied to the structure is displayed in Figure 2-21.

$$T_1 = h_{11} + h_{21} \tag{2.19}$$

$$T_2 = h_{12} + h_{22} \tag{2.20}$$

2.5 Wind Load

A non-linear distributed load is representative of the tower wind load that was calculated using the procedure in Section 2.3.3. This distributed load is converted to the equivalent point load acting at the location z_{bar}, shown in Figure 2-19, which is calculated by setting the sum of the moments equal to zero.

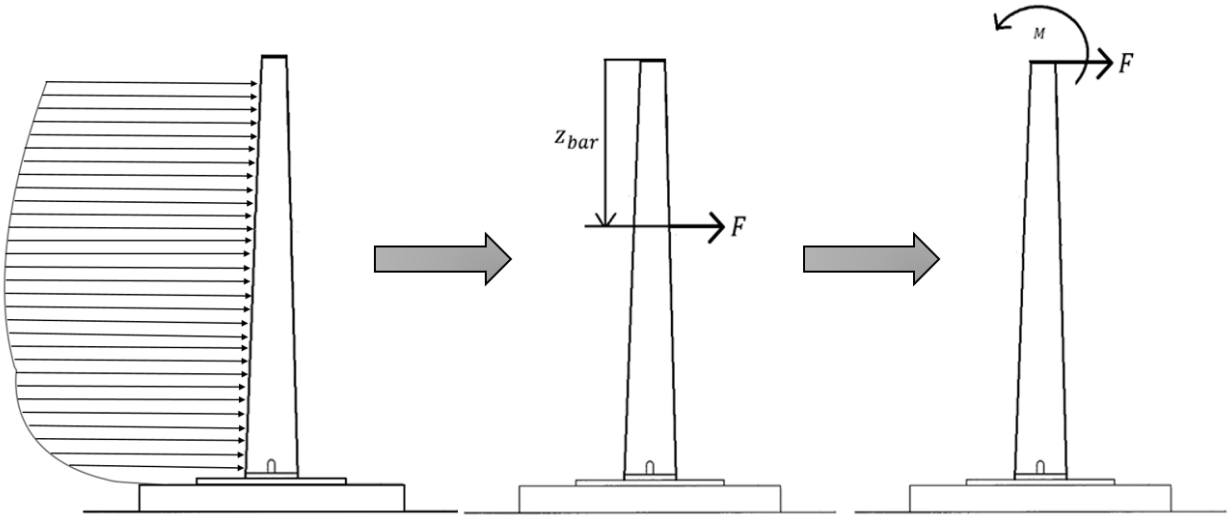

Figure 2-21: Equivalent tower wind load

To allow for free transformation of material due to the constraints, all loading was applied to the top of the tower. When the tower load is applied to the top of the tower, a counteracting moment must be added to remain in static equilibrium. The counteracting moment is the product of the net tower wind load, (F), and the distance that the force acts from hub height (z_{bar}). The values are shown in Table 2-6.

Table 2-6: Table of wind loading and resisting moment

F	1.64 MN
z_bar	68.4 m
M	112 MN*m

The hub height is the height of the center of the rotor. This height is higher than the actual maximum height of the tower. It is assumed that this location also falls at the central horizontal axis of the nacelle, which has a height of 10.5m. This assumption creates a situation where the wind that would hit the top 5m of the tower acts upon the nacelle and nose cone, and the tower experiences no wind load. The wind load experienced at the stall point at each vertical level is shown in Figure A-3.

The equivalent resistant bending moment is applied to the tower in the same manner as the bending moments created by the gravity loads of the turbine components, shown in Figure 2-20.

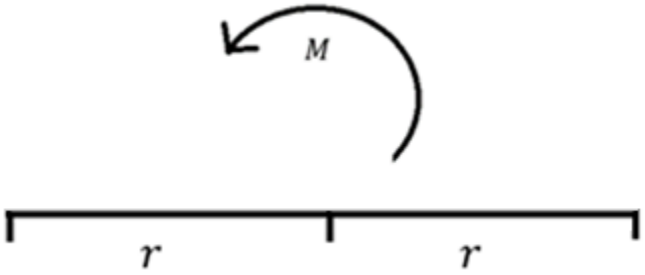

Figure 2-22: Diagram showing the resultant static equivalent bending moment

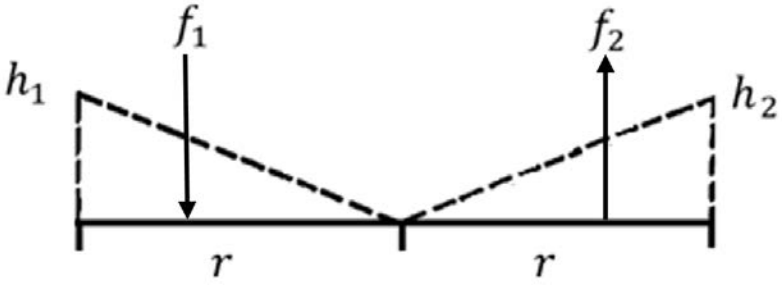

Figure 2-23: Diagram showing distributed loading represented by point loads located at 2/3rds the radius from the tower center

$$0 = f_1 - f_2 \tag{2.21}$$

$$M = f_1 \cdot \frac{2r}{3} + f_2 \cdot \frac{2r}{3} \tag{2.22}$$

2.6 Combined Vertical Loading

The vertical components of the nodal loads applied to the tower model are a combination of the gravity loads of the turbine components, as well as the forces that act as the resisting moment caused by moving the application point of the horizontal wind load of the tower. The calculated combined loading was determined by using a two-dimensional model, with one point at each location of a node in the x-direction. Since the tower is three-dimensional, there are two nodes located at each load point, with the exception of the outer two most nodes of the tower, the applied loading must be halved at each location, and applied to both representative nodes evenly.

Each calculated force is representative of its tributary area. This loading is multiplied by the arc length of the segment of tower that the load represents, determining the equivalent load of the segment. The vertical loading components are broken down and displayed in Figure 2-21 and values are shown in Table A-4. The applied load is shown in more detail in Figure 2-22, and a three-dimensional representation of the loads is found in Figure 2-23. The loading is not to scale, but gives a visual representation of the vertical loading applied to the tower.

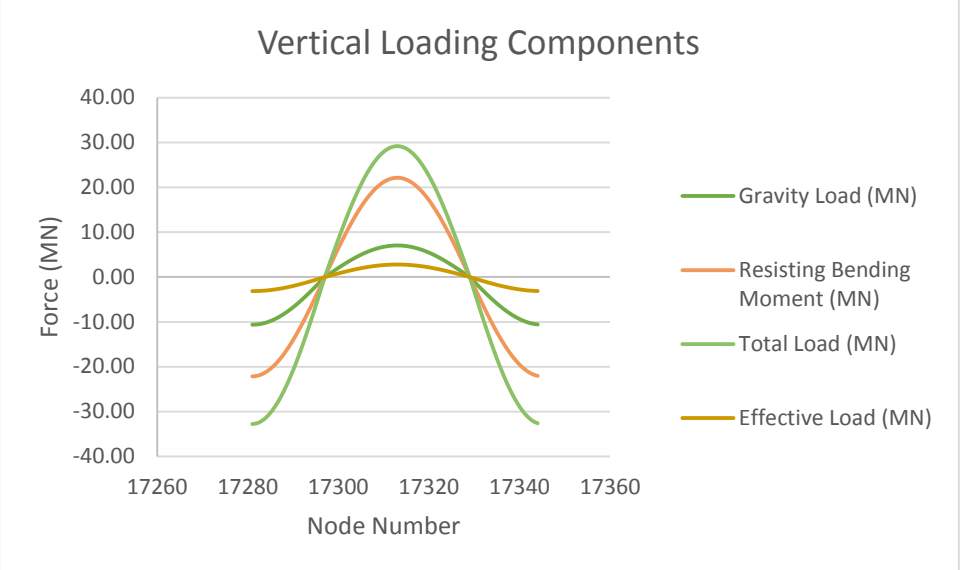

Figure 2-24: Calculated loading on tower nodes

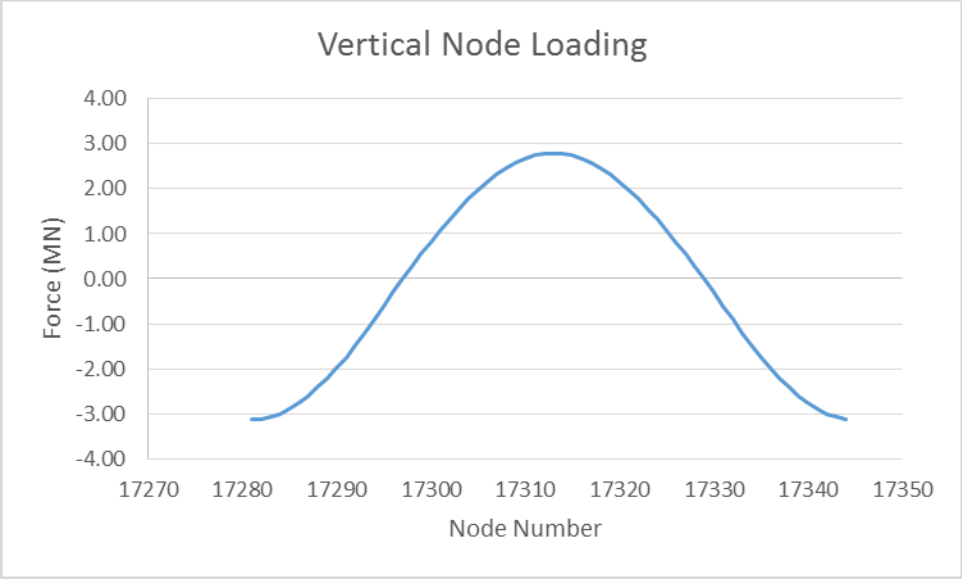

Figure 2-25: Applied loading on tower nodes

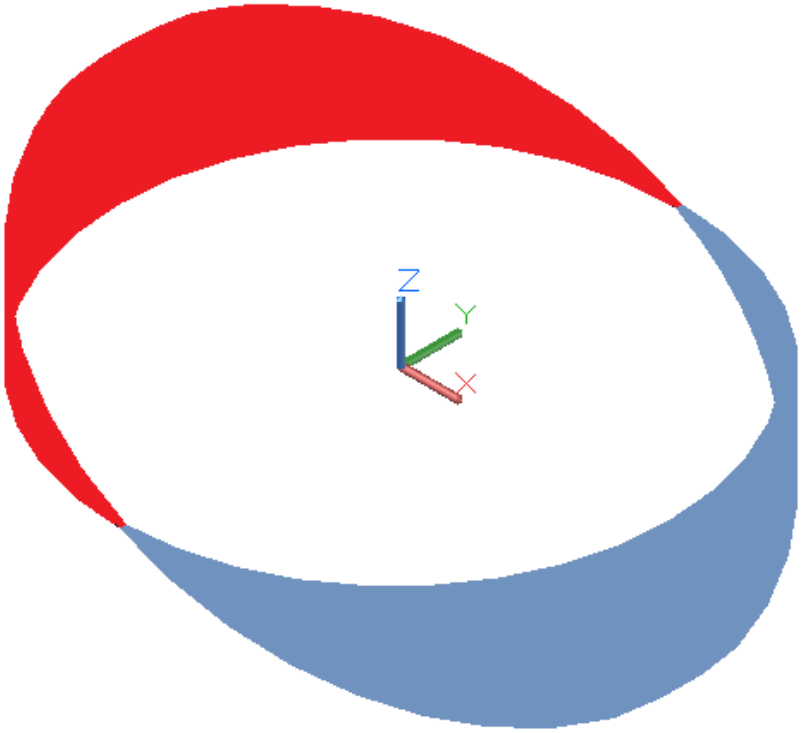

Figure 2-26: Three-dimensional representation of the vertical loading applied

(Red represents compression forces, blue represents tensile forces)

2.7 Combined Horizontal Loading

The total force of the wind loading that acts on the turbine system is applied to the tower as the horizontal component of the force vector. This force is the sum of the wind load that is experienced by the nacelle and nose cone, tower, and drag force on the blades. (Table 2-7)

Table 2-7: Wind loading by component

Total Wind Loads	
Blades	1.56 MN
Nacelle	0.04 MN
Tower	1.64 MN
Total	3.24 MN

CHAPTER 3. OPTIMIZATION PROCESS

3.1 Introduction to Topology Optimization

There are three main approaches used to solve structural optimization problems: size, shape, and topology. Size optimization finds optimal size variables that govern things such as the cross-sectional areas of structural members (Fig 3-1a). Shape optimization finds the variables that govern the boundaries of structural features (Fig 3-1b) while leaving the topology of the system unchanged. Topology optimization (Fig 3-1c) solves for the optimal distribution of material within a structural domain, while allowing the topology (or material connectivity) to vary. The optimal material distribution is often measured by the overall stiffness of the structure where solutions with higher stiffness are favored. Equation Chapter 3 Section 1

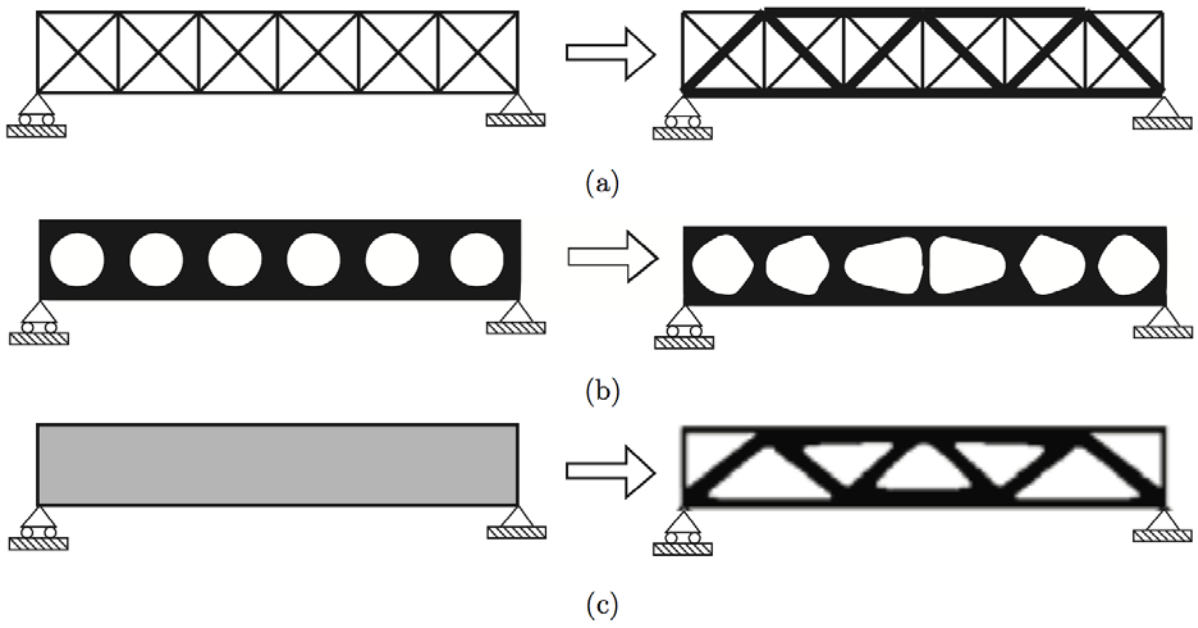

Figure 3-1: Three categories of structural optimization: (a) sizing optimization, (b) shape optimization and (c) topology optimization [3]

Continuum and discrete topology optimization are two approaches to finding the optimal distribution of solid structural material within a set domain. Discrete optimization of a system generally models the structure with distinct elements such as beams, columns, and trusses and often uses a highly connective system of structural members like shown in Figure 3-2 as a starting point to determine the ideal layout of the structure. As the structure is optimized, less

efficient structural members are removed from the ground structure while the more efficient members are retained (al Rabadi, 2014).

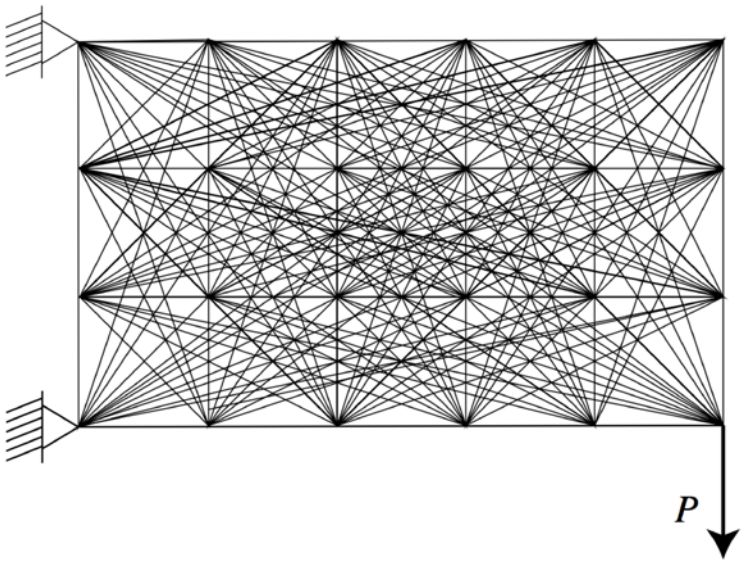

Figure 3-2: Sample ground structure of discrete topology optimization problem [40]

As opposed to discrete structural topology optimization which uses truss and beam-column structural members, continuum topology models are based on more fundamental solid continuum mechanics models. One generally begins with a fixed spatial domain and seeks the optimal distribution of solid structural within this domain. This is achieved by parameterizing the porosity of the structural material throughout the domain. In the end, regions of the structural domain that have complete porosity will be devoid of structural material, while regions that have vanishing porosity will be completely solid.

3.2 Bilinear Shell Finite Element

The finite elements that are used to create the structural model are bilinear continuum shell elements. These elements possess five degrees of freedom, and are used to solve three-dimensional static or dynamic equilibrium problems over the structural domain. The element geometry as displayed in Figures 3-3 and 3-4 can be described by the Eq. (3.1).

$$\mathbf{X}(\xi,\eta,\zeta)=\sum_{A=1}^{n_{en}} N_A(\xi,\eta)\left[\bar{\mathbf{X}}_A+z_A(\zeta)\hat{\mathbf{X}}_A\right] \tag{3.1}$$

where, n_{en} is the number of elemental nodes, and N_A is the shape or interpolation function of the A^{th} elemental node, and $\hat{\mathbf{X}}_A$, is a unit vector aligned with the nodal fiber:

$$\hat{\mathbf{X}}_A = \frac{\mathbf{X}_A^+ - \mathbf{X}_A^-}{\left\|\mathbf{X}_A^+ - \mathbf{X}_A^-\right\|} \tag{3.2}$$

For a given node A, $\mathbf{X}_A^+$ marks the top surface of the shell $(\zeta = +1)$, $\mathbf{X}_A^-$ marks the bottom surface of the shell $(\zeta = -1)$ and $\bar{\mathbf{X}}_A$ marks the reference surface $(\zeta = \bar{\zeta})$. The thickness function, $z_A(\zeta)$ at each node is defined as:

$$z_A(\zeta) = \frac{1}{2}(\zeta - \bar{\zeta})\left\|\mathbf{X}_A^+ - \mathbf{X}_A^-\right\| \tag{3.3}$$

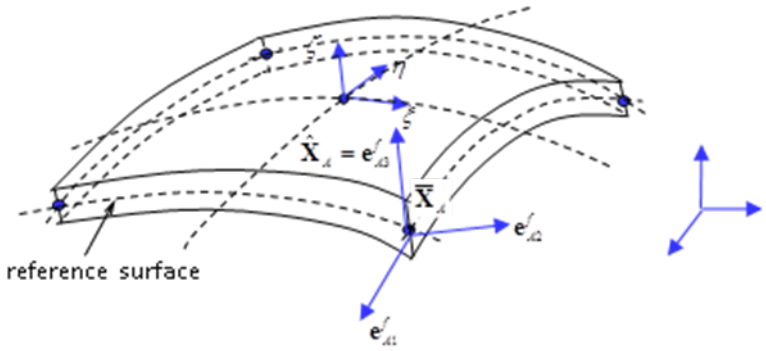

Figure 3-3: Geometric description of the shell element

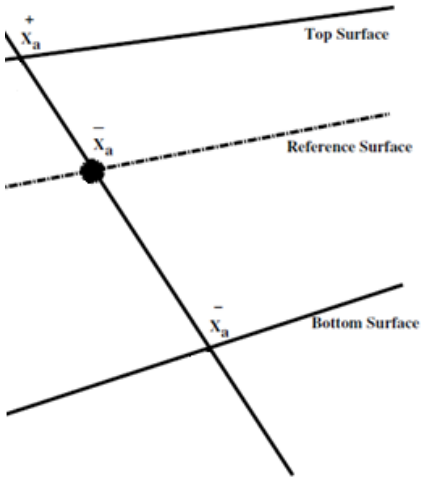

Figure 3-4: Relative nodal points

Since the shell domain of the structure is discretized into a mesh consisting of finite elements, the elements must be able to take general shapes. The displacement field within an element uses the same interpolation functions as those used in the definition of the nodal points.

$$\mathbf{u}(\xi,\eta,\zeta) = \sum_{A=1}^{n_{en}} N_A(\xi,\eta)\left[\bar{\mathbf{u}}_A + z_A(\zeta)\hat{\mathbf{u}}_A\right] \tag{3.4}$$

where, $\bar{\mathbf{u}}_A$ represents the reference surface nodal translation at the node A, and $\hat{\mathbf{u}}_A$ is the nodal rotations as described by Hughes (1987).

The expression of equilibrium in a small deformation Lagrangian function, is written for all points **X** that fall within the reference configuration (Ω):

$$\sigma_{ji,j} + \rho\, b_i = 0 \;\forall \mathbf{X} \;\in \Omega \tag{3.5}$$

where σ_{ji} is the Cauchy stress tensor, ρ is the mass density, and **b** is the gravitational acceleration vector.

The internal virtual work done by the internal stresses $\left(\delta W^{\text{int}}\right)$ is represented by Eq. (3.6) while the external virtual work performed by applied surface tractions and gravity loading is expressed in Eq. (3.7).

$$\delta W^{int} = \int_{\Omega} (\delta\varepsilon_{ij})\sigma_{ji}\, d\Omega \tag{3.6}$$

$$\delta W^{ext} = \int_{\Gamma} \delta u_i n_j \sigma_{ji}\, d\Gamma + \int_{\Omega} \delta u_i \rho b\, d\Omega \tag{3.7}$$

The principal of virtual work yields equality of the internal and external virtual work expressions, and leads ultimately to expressions for nodal internal forces, nodal external forces associated with traction and gravity loads, and the nodal stiffness matrices which when assembled yield the global stiffness matrix. In Eq. (3.6), the internal stresses are obtained by linear elasticity (Hooke's Law). Small strains and rotations are assumed in the analysis so that:

$$\varepsilon_{ij} = \frac{1}{2}\left(u_{i,j} + u_{j,i}\right) \text{ and } \delta\varepsilon_{ij} = \frac{1}{2}\left(\delta u_{i,j} + \delta u_{j,i}\right) \tag{3.8}$$

3.3 Volume Fraction

The structural domain is composed of a mesh of *NEL* non-overlapping bilinear continuum degenerated shell finite elements, with each element having *nen* nodes. Each element contains a spatially varying amorphous mixture of materials A and B. [For the application at hand, material *A* represents the primary structural material of which the wind turbine tower is constructed (i.e. structural steel) and material *B* is a void-like material having negligible stiffness and mass density.] At any given point **X** within a shell finite element, the volume fraction of material, *A* is obtained as a spatial interpolation of the volume fractions of material A at the element nodes.

$$\text{for } \mathbf{X} \in \Omega_e, \qquad \phi_A(\mathbf{X}) = \sum_{I=1}^{nen} N_I^e(\mathbf{X})\phi_{AI} \tag{3.9}$$

where Ω_e is the domain of the eth finite element, $N_I^e(\mathbf{X})$ is the I^{th} shape function of the e^{th} element and ϕ_{AI} is the volume fraction of material *A* at the I^{th} node. At any point **X** in the structural model, the volume fractions of materials A and B sum to unity as follows:

$$\phi_A(\mathbf{X}) + \phi_B(\mathbf{X}) = 1 \quad \text{for all } \mathbf{X} \in \Omega \tag{3.10}$$

The structural design space is represented by a vector, which is comprised of the volume fraction of each node.

$$\mathbf{b}_i = \left\{\phi_1, \phi_2, \phi_3, \phi_4, ..., \phi_{n_{dv}}\right\} \tag{3.11}$$

In Eq. (3.11), n_{dv} is the number of design variables in the total system. $\phi_n \in (0,1)$, where 1 represents a solid structural material, and 0 represents a void space.

At the beginning the entire design domain modeled as a solid function represented by the vector $\mathbf{b}_o$.

$$\mathbf{b}_o = \{1,1,1,1,...,1\} \tag{3.12}$$

3.4 Topology Optimization Mixing Rules

To characterize the stiffness of an amorphous mixture of materials A and B, different so-called mixing rules are often employed. In the Voigt rule of mixtures, it is assumed that the materials *A* and *B* share the same state of strain. Consequently, the effective elasticity tensor for a mixture of two linear elastic materials A and B with respective volume fractions ϕ_A and ϕ_B is given by the following relation:

$$\left(\mathbf{E}^*\right)^{Voigt} = \phi_A \mathbf{E}^A + \phi_B \mathbf{E}^B \tag{3.13}$$

where $\mathbf{E}^A$ is the stiffness tensor or matrix of material *A*, and $\mathbf{E}^B$ that of material *B*. Alternatively, under the Reuss isostress assumption, the effective elasticity tensor of the mixture would be

$$\left(\mathbf{E}^*\right)^{Reuss} = \left[\phi_A \left(\mathbf{E}^A\right)^{-1} + \phi_B \left(\mathbf{E}^B\right)^{-1}\right]^{-1} \tag{3.14}$$

With $\left\|\mathbf{E}^A\right\| >> \left\|\mathbf{E}^B\right\|$, the Reuss rule is essentially discontinuous at $\phi_A = 1$ (Figure 3.5). This can be remedied somewhat by using hybrid Voigt-Reuss mixing rules of the form:

$$\left(\mathbf{E}^*\right)^{hybrid} = \alpha \left(\mathbf{E}^*\right)^{Voigt} + (1-\alpha)\left(\mathbf{E}^*\right)^{Reuss} \tag{3.15}$$

with $\alpha \in [0,1]$. Nevertheless, even with $\left\|\mathbf{E}^A\right\| >> \left\|\mathbf{E}^B\right\|$ the hybrid rule is still essentially discontinuous at $\phi_A = 1$. While the Reuss rule of mixtures is potentially quite useful when designing the layout of two solids with moduli that are relatively close to one another (i.e. within a factor of 100) as in the design of material arrangement within a composite unit cell [60], it is less suited to applications involving solid and void materials.

A mixing rule more suitable for solid-void mixtures is the so-called powerlaw mixing rule, first investigated by Bendsøe (1989), having the form:

$$\left(\mathbf{E}^*\right)^{powerlaw} = \left(\phi_A\right)^p \mathbf{E}^A + \left[1-\left(\phi_A\right)^p\right]\mathbf{E}^B \tag{3.16}$$

for $p \geq 1$. For $p = 1$, the powerlaw rule recovers the Voigt rule of mixtures. Nevertheless, the powerlaw mixing rule does not recover the Reuss mixing rule in any limit. The relative characteristics of each of these mixing rules and also homogenization of a periodic porous solid are displayed in Figure 3.5.

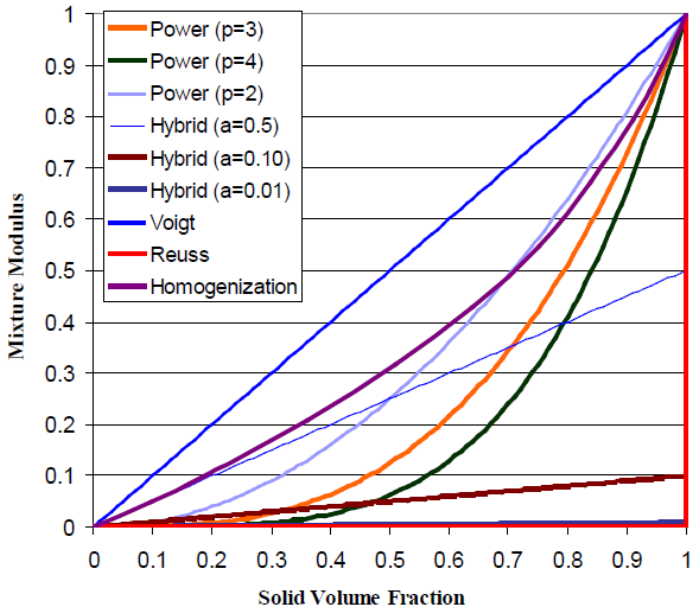

*Figure 3-5:Plot of mixture modulus versus solid volume fraction for various mixing rules including the Voigt, Reuss, and hybrid rules, and the powerlaw rule. The formulae were applied with E^A=1.0 and E^B=1.0*10^{-6}[60]*

A relatively common design goal in continuum structural topology optimization is to find the arrangement of a constrained amount of structural material having specified properties that minimizes the structural compliance with respect to the applied loading. The applied loading can be from external forces such as point loads, tractions, and body forces, and from applied displacements. For such a problem, the design optimization problem could be stated as follows:

$$\min_{\mathbf{b}} \left[M(\mathbf{u},\mathbf{b}) = \tfrac{1}{2} \left(\mathbf{f}^{ext} \cdot \mathbf{u} + \sum_{E \in \eta_g} \mathbf{f}_E^{\text{int}} \cdot \mathbf{g}_E \right) \right] \tag{3.17a}$$

such that:

$$\mathbf{r}(\mathbf{u},\mathbf{b}) = 0 \tag{3.17b}$$

$$\frac{1}{V}\int_{\Omega}\phi_A \, d\Omega - C \leq 0 \tag{3.17c}$$

$$b_L \leq b_i \leq b_U \quad i \in \{1,2,\ldots,n_{dv}\} \tag{3.17d}$$

Above, $\mathbf{u} \in \Re^{NEQ}$ represents a vector of nodal displacements where NEQ is the number of unknowns in the structural analysis problem, and $\mathbf{g}_E$ for $E \in \{\eta_g\}$ represent specified displacements applied to the structure. In the equality constraint of Eq. (3.17b) $\mathbf{r} \in \Re^{NEQ}$ is the vector of unbalanced forces at each unrestrained node in the model, and the condition that $\mathbf{r} = \mathbf{0}$ states that under the applied loading the structure must be in a state of minimum potential energy. The inequality constraint of Eq. (3.17c) imposes an upper bound on the volume of structural material that can be used (i.e. $C \cdot V$) where $C \in (0,1)$ and V denotes the volume of the structural domain Ω Finally, Eq. (3.17d) represents bounds on the continuous values that can be taken by individual design variables, and n_{dv} denotes the number of design variables in the optimization problem.

In structural compliance minimization problems such as this, the nature of the design solutions obtained will depend in large measure upon how the mixtures of solid and void are treated. The Voigt rule of mixtures assigns to any mixture of solid and void with a specific solid volume fraction, the highest possible stiffness that is physically achievable. Accordingly, if the Voigt rule of mixtures is used in solving for the stiffest possible layout of material on the structural scale, the optimum would have a strong tendency to feature mixtures of materials (or composites). In this sense, it would be said that the Voigt rule of mixtures does not penalize mixtures.

On the other extreme, for a solid-void mixture with a specific solid volume fraction, the Reuss rule of mixtures will assign to that mixture the lowest physically realizable stiffness. With the Reuss treatment of mixtures, it is thus unlikely that mixtures would be utilized in the final design, since they are extremely compliant. Restated, with the Reuss treatment, mixtures or composites pay a severe performance penalty in terms of stiffness.

There are numerous treatments of mixtures/composites intermediate to those of the Voigt and Reuss rules of mixtures that provide varying degrees of penalization (Figure 3.5). The

homogenized structured porous solid composite treatment of mixtures is slightly more penalized, in terms of stiffness, than the Voigt rule of mixtures, and comparable at high solid volume fractions to the powerlaw mixing rule with $p = 2$. The powerlaw mixing rules with $p = 3$ and $p = 4$, respectively, are strongly penalized in terms of stiffness and thus when used in compliance minimization problems, tend to yield designs that do not use mixtures.

While solving continuum structural topology optimization problems using penalized mixing rules leads to concept designs that are more representative of those used in real word applications (i.e. black and white with negligible regions containing mixtures, it will likely not achieve the global minimum compliance. Penalized structures tend to have many local minima, and have a higher compliance because of the elimination of partially solid elements (Figure 3-6).

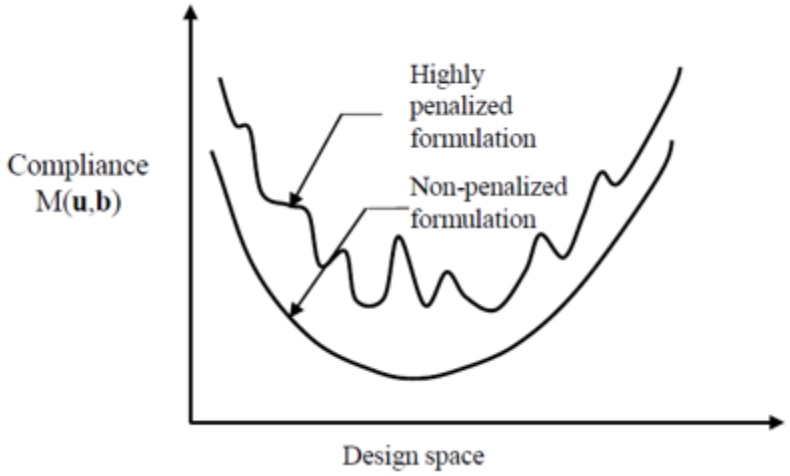

Figure 3-6: Comparison between the compliance of non-penalized systems, and highly penalized systems [61]

For all homogenization treatments and mixing rule treatments of two solids A and B, the mass density (ρ) of the mixtures is always computed in the same manner:

$$\rho = \phi_A \rho_A + \phi_B \rho_B \tag{3.17}$$

While different treatments of mixtures may lead to varying degrees of penalization of the stiffness, there is only one treatment of the effective mass density and this involves no penalization.

3.5 Sensitivity Analysis

The sensitivity analyses checks the finite difference of the design objective and constraint gradient vectors with a specified starting step size, against updated step sizes. When gradient based optimization methods are used to solve continuum structural topology design problems, the ability to determine the derivatives of the design functions is crucial. In compliance minimization problems the derivative of the compliance function (M(**u**,**b**)), with respect to the design vector ($\mathbf{b}_i$) is calculated.

$$\frac{dM}{d\mathbf{b}} = \frac{1}{2}\left(\frac{d\mathbf{F}^{\mathbf{ext}}}{d\mathbf{b}} \cdot \mathbf{u} + \mathbf{F}^{\mathbf{ext}} \cdot \frac{\partial \mathbf{u}}{\partial \mathbf{b}} \right) \tag{3.18}$$

Since $\mathbf{F}^{\text{ext}}$ is a vector of constants and not dependent on the design vector, Eq. (3.19) can be simplified to Eq. (3.20).

$$\frac{dM}{d\mathbf{b}} = \frac{1}{2}\mathbf{F}^{\mathbf{ext}} \cdot \frac{\partial \mathbf{u}}{\partial \mathbf{b}} \tag{3.19}$$

The evaluation of a system at static equilibrium, potential energy is represented in terms of internal and external forces as:

$$\mathrm{r}(\mathbf{b},\mathbf{u}) = \mathbf{F}^{int} - \mathbf{F}^{ext} = 0 \tag{3.20}$$

For a structure experiencing a linear elastic response behavior the relationship between the applied external loads and the resulting displacement can be represented as:

$$\mathrm{r}(\mathbf{b},\mathbf{u}) = \mathbf{K} \cdot \mathbf{u} - \mathbf{F}^{ext} \tag{3.21}$$

In the equation **K** is the stiffness of the structure, **u** is the vector of nodal displacements and $\boldsymbol{F}^{ext}$ is a vector of external forces acting on the system.

The derivative of Eq. (3.22) in respect to the design vector (**b**), for a system at an equilibrium state is:

$$\frac{d\mathbf{r}}{d\mathbf{b}} = \frac{d\mathbf{K}}{d\mathbf{b}} \cdot \mathbf{u} - \mathbf{K} \cdot \frac{d\mathbf{u}}{d\mathbf{b}} = 0 \tag{3.22}$$

Eq. (3.23) when solved for the derivative of the displacement vector in respect to the design vector is:

$$\frac{d\mathbf{u}}{d\mathbf{b}} = -\mathbf{K}^{-1} \cdot \frac{d\mathbf{K}}{d\mathbf{b}} \cdot \mathbf{u} \tag{3.23}$$

Substituting Eq. (3.23) into Eq. (3.20) simplifies to:

$$\frac{dM}{d\mathbf{b}} = -\frac{1}{2}\mathbf{F}^{\mathbf{ext}} \cdot \mathbf{K}^{-1} \cdot \frac{d\mathbf{K}}{d\mathbf{b}} \cdot \mathbf{u} \tag{3.24}$$

By solving Eq. (3.22) for $\mathbf{F}^{\text{ext}}$ and substituting into Eq. (3.25), the equation can be simplified to:

$$\frac{dM}{d\mathbf{b}} = -\frac{1}{2}\mathbf{u} \cdot \frac{d\mathbf{K}}{d\mathbf{b}} \cdot \mathbf{u} \tag{3.25}$$

Substituting Eq. (3.22) into Eq. (3.21) and solving for $\mathbf{F}^{\text{int}}$, Eq. (3.26) can be simplified further to Eq. (3.28).

$$\mathbf{F}^{\text{int}} = \mathbf{K} \cdot \mathbf{u} \tag{3.26}$$

$$\frac{dM}{d\mathbf{b}} = \mathbf{u}^{a} \cdot \frac{\partial F^{\text{int}}}{\partial \mathbf{b}} \tag{3.27}$$

where $\mathbf{u}^{a} \in \Re^{NEQ}$ is the vector of adjoint displacement vector, which satisfies Eq. (3.29).

$$\mathbf{K} \cdot \mathbf{u}^{a} = -\frac{\partial M}{\partial \mathbf{u}} = -\frac{1}{2}\mathbf{F}^{ext} \tag{3.28}$$

Which results in an adjoint displacement vector where:

$$\mathbf{u}_{a} = -\frac{1}{2}\mathbf{u} \tag{3.29}$$

The internal forces in the system can be represented by Eq. (3.31), where **B** represents the strain displacement matrix. σ and ε are stress and strain vectors respectively.

$$\sigma = (\sigma_{11}, \sigma_{22}, \sigma_{33}, \sigma_{23}, \sigma_{13}, \sigma_{12})$$

$$\varepsilon = (\varepsilon_{11}, \varepsilon_{22}, \varepsilon_{33}, \gamma_{23}, \gamma_{13}, \gamma_{12})$$

$$\mathbf{F}^{\text{int}} = \int_{\Omega} \mathbf{B}^T \boldsymbol{\sigma} d\Omega \tag{3.30}$$

Using Hooke's Law, Eq. (3.31), can be expressed as Eq. (3.32), where **E**(b) is the elasticity tensor.

$$\mathbf{F}^{\text{int}} = \int_{\Omega} \mathbf{B}^T \mathbf{E}(b) \cdot \boldsymbol{\varepsilon} d\Omega \tag{3.31}$$

Substituting Eq. (3.32) into Eq. (3.28), the derivative of the structural compliance can be expressed in terms of strains.

$$\frac{dF}{d\mathbf{b}} = \mathbf{u}^a \cdot \frac{\partial}{\partial \mathbf{b}} \left(\int_{\Omega} \mathbf{B}^T \mathbf{E}(b) \cdot \boldsymbol{\varepsilon} d\Omega \right) \tag{3.32}$$

$$\frac{dF}{d\mathbf{b}} = \mathbf{u}^a \cdot \left(\int_{\Omega} \mathbf{B}^T \frac{\partial \mathbf{E}(b)}{\partial \mathbf{b}} \cdot \boldsymbol{\varepsilon} d\Omega \right) \tag{3.33}$$

When it is assumed that the external loading ($\mathbf{F}^{\text{int}}$) is independent to the design variables the equation reduces to:

$$\frac{dF}{d\mathbf{b}} = \int_{\Omega} \boldsymbol{\varepsilon}_a \cdot \frac{\partial \mathbf{E}(b)}{\partial \mathbf{b}} \cdot \boldsymbol{\varepsilon} d\Omega \tag{3.34}$$

An important aspect of the process of solving this optimization problem was to check that the derivative of the design functions are calculated correctly as the design space was updated. The program was modified to solve three dimensional shell elements, and it was necessary to check that the program progresses as expected. A program was written where the slope of the design functions were determined and analyzed. An initial design vector (**b**) was input for a test bilinear shell element model, and a finite element analysis was performed. The values of the design functions for the solution of the problem was exported and the design vector was updated by a specified amount. A finite element analysis was performed on the updated model and the solution exported. The two solutions were scaled from the change in the design vector to determine the design gradient for the system.

$$\frac{dF}{d\mathbf{b}} = \frac{F_i - F_{i-1}}{\mathbf{b}_i - \mathbf{b}_{i-1}} \tag{3.35}$$

The calculated design gradient was checked against the design gradient that was solved for by the finite element program, to perform a sensitivity analysis check on the program. Since the design gradient is determined for each design variable in the system, $\frac{dF}{d\mathbf{b}}$ is a vector with a length that is the same as the number of design variables. To compare the two vectors, the finite difference analyses of the two vectors was performed. The analysis compared length and the normalized dot product of the vectors to determine if the program solution, matched the calculated.

3.6 Continuum Topology Optimization Procedure

The continuum topology optimization process is iterative, requiring the problem to be solved with each variation in the design. There are nine operations that occur in the optimization process, which can be grouped into four procedural steps. The process minimizes the objective function(s), subject to the constraint function(s).

The step-by-step optimization process described is laid out in Figure 3-7, where k is the number of iterations.

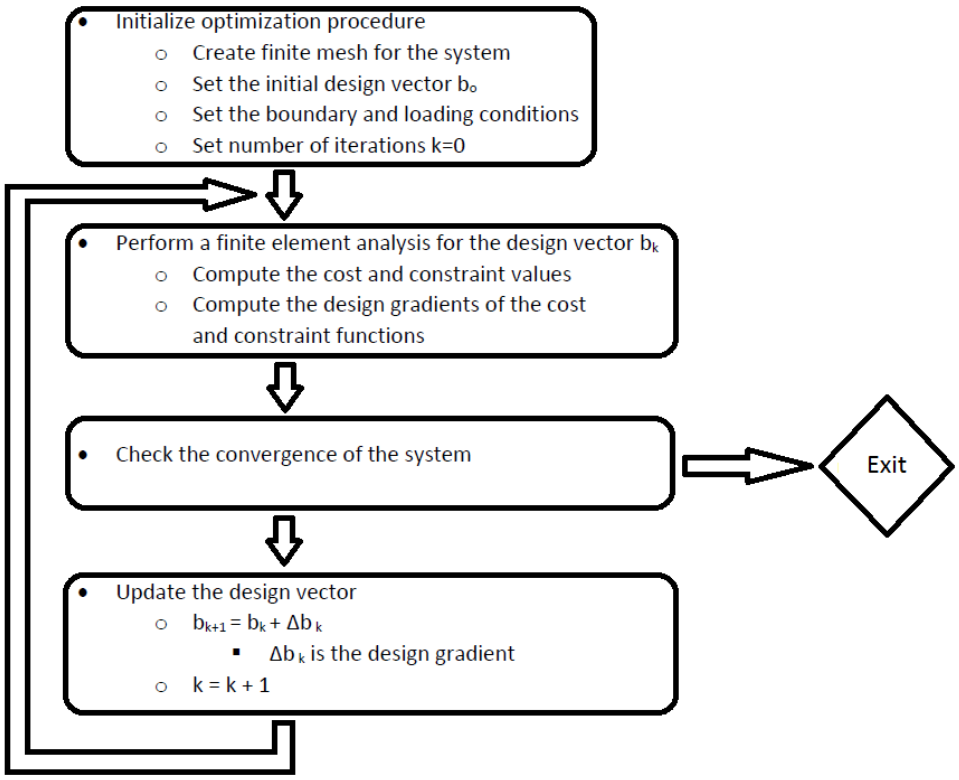

Figure 3-7: Flowchart of the topology optimization procedure

The first step in the optimization process is to create a mesh of finite elements representative of the structural system, and creating a system of boundary conditions and loads.

The optimization procedure then progresses into a loop, which begins by evaluating the equilibrium equations by performing finite element analysis (FEA) on the initial design. The next step is to preform sensitivity analysis calculations to compute the derivative of the objective and constraint functions, and their design gradients. Initially a set step size is used to update the design vector. After the first iteration, the design vector can be updated using gradient-based optimization procedures. If, after an iteration, the convergence criteria has not been met, or the specified maximum number of iterations has not yet been performed, the gradient of the change in compliance and the change in the design space are used to update the system and create a new design vector ($\mathbf{b}_{i+1}$). A new finite element analysis is performed on the updated system, and when the current design reaches the optimal solution under the prescribed criteria, the iterative process ends and the optimum material layout for the system under the design criteria has been determined.

The optimization process employs the use of mathematical programming to minimize the compliance of the system subject to the constraints. Sequential linear programming algorithms (SLP) are used as the mathematical process to solve this problem, because of its efficiency for solving nonlinear problems with a large number of design variables. SLP works by solving a series of linear sub-problems through the creation of linear Taylor series expansions for the dependent functions.

SLP uses a set of input data as in addition to the data it imports from the finite element analysis and model mapping. The algorithms use an input of: the number of design variables, number of equality and inequality constraints, a set of convergence criteria, a move limit, and the hybridization parameter.

The process of the SLP algorithm, follows the steps described by Mijar. [34]

Step 1: Collect input data, and set initiation criteria.

- Set iteration counter k=0
- Initialize a staring design ($\mathbf{b}^{(0)}$) and select move limit.
- Specify stopping criteria for both equality and inequality constraints, as well as the design vector.

Step 2: Evaluate the cost and constraint functions and their gradients at the current design point ($\mathbf{b}^{(k)}$).

Step 3: Solve for the maximum constraint violation at the current design point. Check for convergence with the stopping criteria for the maximum constrain violation.

Step 4: Solve for the norm of the design vector at the current iteration. Check for convergence with the criteria for the design vector.

Step 5: Solve the LP sub-problem for the search direction $\mathbf{d}^{(k)}$.

Step 6: Use line search to find a step size that meets the decent criteria for:

$$\Delta \mathbf{b}^{(k)} = \alpha_k \mathbf{d}^{(k)} \tag{3.36}$$

Step 7: Check for convergence. If the maximum constrain violation and the change in the design vector meet convergence criteria then problem stops.

Step 8: If convergence criteria are not met then the design vector and iteration counter are updated.

$$\mathbf{b}^{(k+1)} = \mathbf{b}^{(k)} + \Delta \mathbf{b}^{(k)} \tag{3.37}$$

In order to conserve resources, a maximum number of iterations can be implemented to ensure that a stopping point for the program if the convergence criteria are not met in a reasonable amount of time. A move limit is implemented to be used as the initial step size as well as ensuring that the gradient determined step size, is not too large and skips over potential optimal solutions. [3]

3.7 Symmetry Planes

Symmetry planes are used to enforce geometric symmetry constraints on the layout of the design. The symmetry planes work by providing information that is used to map the correspondence between finite elements of the structural model and their design variables. For each symmetry plane implemented the number of design variables used in the solution of the finite element model is approximately halved. Symmetry is critical for the design of the material layout of the turbine tower because of the variability of the wind direction. To limit the effect that the direction of the wind would have on the tower, four symmetry planes were implemented, dividing the tower into eight equal sections.

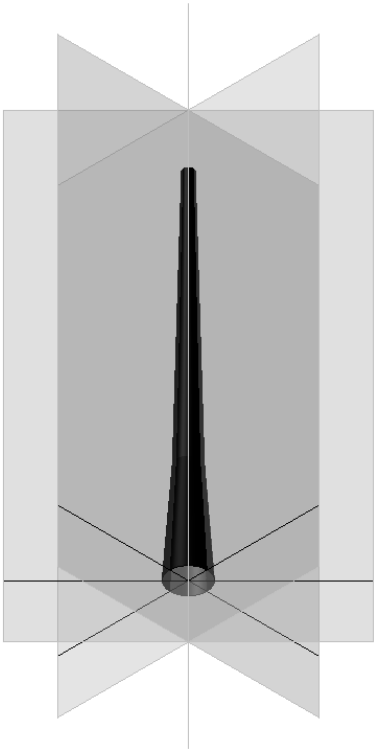

Figure 3-8: Visual representation of the symmetry planes applied to the tower model

3.8 Sample Optimization Problem

An optimization problem of a simply supported beam system shown in Figure 3-6, was solved in order to test the optimization procedure on a two dimensional problem. The sample problem was also able to look into one of the shortfalls of using the optimization procedure, the production of mesh dependent solutions. While this aspect did not come into play in the tower optimization problem, the two dimensional problem provided the ability to have a gradual introduction into the software through the solution of a more simple problem, shown in Figure 3-6. The point load that is applied to the structure is 100 units of force. The structure is 120 units wide by 20 units tall, creating a course mesh of one-unit square elements, a midrange mesh of quarter square unit elements, and dense mesh of one-sixteenth unit elements.

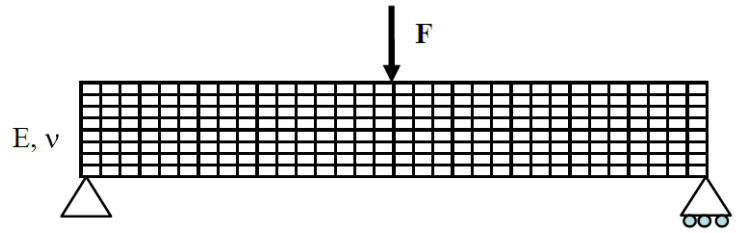

Figure 3-9: Diagram of the design of the beam structure undergoing optimization [61]

There are two sets of design criteria that were used to solve the beam system. The first used the design criteria of force-controlled strain energy minimization, and having a global volume fraction that was less than or equal to 25 percent of the original volume. The second solved the optimizing problem by using the same two criteria as part one, but also added a perimeter constraint. To analyze the convergence of each set of design criteria, the system was solved at three different mesh densities. The coarsest mesh was 120x20, the middle was 240x40, and the finest mesh had a density of 480x80 units.

Perimeter control is a commonly used constraint function that implements a limitation on the "fineness" of the system. This is used to obtain convergence of the material layout designs with mesh refinement. The process of implementing a perimeter constraint into the optimization process was introduced in Haber (1996). It features the employment of a maximum value of the calculated surface area of the material sub-units, to limit material placement, and favor solutions with fewer distinct features. [60]

Solving the beam problem without the perimeter constraint for the three different mesh densities resulted in different optimized solutions, which did not converge to a single material layout, but instead developed more detail as the mesh became finer.

When the perimeter constraint used in the optimization process, $P(b) - Pu \leq 0$ where Pu $= 2(\text{length} + \text{height})$, was added to the design criteria, the material layout converged to one material layout.

The final material layouts for the system when optimized using the two different design criteria are shown in Figures 3-10, 3-11 and 3-12. These figures show how as the mesh density increases; the optimum solutions develop finer detail. These contrasts to the final material

layouts for the design space when the perimeter constraint is added to the system, which all have very similar solutions.

Figure 3-10: 120x20 mesh without perimeter constraint (left), with perimeter constraint (right)

Figure 3-11: 240x40 mesh without perimeter constraint (left), with perimeter constraint (right)

Figure 3-12: 480x80 mesh without perimeter constraint (left), with perimeter constraint (right)

Each of the optimum solutions shown has their own compliance (cost function). The goal is to minimize the compliance of the structure while meeting the constraint criteria. As the meshes get finer the stiffness of the system slightly increases, the results shown in Table 3-1. The increased stiffness is caused by the addition of small details that are able to be included because the finer mesh can show more detail.

Table 3-1: Compliance of the different mesh sizes and constraint conditions

Compliance		
	Perimeter Constraint	No Perimeter Constraint
120x20	4560	3790
240x40	3570	3310
480x80	3130	2850

Performing topology optimization on the simply supported beam problem, with an external loading allowed for an introduction into the optimization procedure. The knowledge gained from solving this problem aided in the attempt to solve the more complicated tower problem.

CHAPTER 4. OPTIMIZATION PROBLEM SET UP

4.1 Tower Model

The tower model consists of a mesh comprised of 64 bilinear shell elements per half-meter tall cross-sectional ring, for a total of 17,280 elements, 17,344 nodes, 2439 design variables and 12,195 degrees of freedom.

The tower is 135m tall, has a maximum diameter of 14.5m, and a uniform thickness of 20cm. The initial design has a total volume of 2752m^3 of structural steel.

Nodal forces are applied to the each node that makes up the top edge of the mesh. The model uses nodal forces to represent the equivalent loading experienced by the turbine. These forces are applied as three-dimensional vectors, and therefore can be used to represent the vertical gravity loads as well as the horizontal wind loading.

4.2 Material Properties

The tower of the wind turbine model is produced using elements with the material properties of structural steel members, shown in Table 4-1. While the Enercon E-126 tower is constructed out of precast concrete segments, the model uses structural steel as the solid material. Structural steel allows for more flexibility and a shorter construction process at a reduced cost. By using prefabricated structural steel framing the overall cost of the tower can be reduced by 2-3% or more, when compared to an equivalent structure of reinforced concrete.

Table 4-1: Material properties

Structural Steel Material Properties	
Material Mass Density	7900 kg/m^3
Young's Modulus	24.16 GPa
Shear Modulus	11.15 GPa

To provide the material used for the tower model with the properties of structural steel, it is assigned the mass density, shear and Young’s moduli, as well as the 21 independent elastic moduli.

Hooke's law assumes that the components of the stress tensor are linear functions of the strain tensor. This allows for there to be a relationship between the stresses and the gradient of deformation that occurs in the material.

The compliance matrix enables stresses to be converted into strains. The inverse of the compliance matrix, known as stiffness matrix allows to solve in the other direction, and is the input for the material matrix for the finite element program.Equation Chapter (Next) Section 1

The Hooke's Law for an isotropic elastic material is:

$$\begin{pmatrix} \epsilon_x \\ \epsilon_y \\ \epsilon_z \\ \gamma_{xy} \\ \gamma_{yz} \\ \gamma_{xz} \end{pmatrix} = \begin{pmatrix} \frac{1}{E} & \frac{-\nu}{E} & \frac{-\nu}{E} & 0 & 0 & 0 \\ \frac{-\nu}{E} & \frac{1}{E} & \frac{-\nu}{E} & 0 & 0 & 0 \\ \frac{-\nu}{E} & \frac{-\nu}{E} & \frac{1}{E} & 0 & 0 & 0 \\ 0 & 0 & 0 & \frac{1}{G} & 0 & 0 \\ 0 & 0 & 0 & 0 & \frac{1}{G} & 0 \\ 0 & 0 & 0 & 0 & 0 & \frac{1}{G} \end{pmatrix} \cdot \begin{pmatrix} \sigma_x \\ \sigma_y \\ \sigma_z \\ \tau_{xy} \\ \tau_{yz} \\ \tau_{xz} \end{pmatrix} \tag{4.1}$$

The steel used in the design has the properties shown in Table 4-1. By modeling the tower as a structure constructed out of an isotropic elastic material, the stiffness matrix can be represented as the matrix, S_{ij}, all values are in GPa.

$$S_{ij} = \begin{pmatrix} 269 & 115 & 115 & 0 & 0 & 0 \\ 115 & 269 & 115 & 0 & 0 & 0 \\ 115 & 115 & 269 & 0 & 0 & 0 \\ 0 & 0 & 0 & 76.9 & 0 & 0 \\ 0 & 0 & 0 & 0 & 76.9 & 0 \\ 0 & 0 & 0 & 0 & 0 & 76.9 \end{pmatrix} \tag{4.2}$$

The void material is assumed to have properties one trillionth that of the solid material. This allows the program to use minuscule strengths for voids, which avoids indeterminate expressions occurring in the computing functions.

4.3 Bottom Tower Restraint

The nodes at bottom of the tower are restrained in all directions to create a simulated fixed foundation. The restrained nodes provide support for the structure which maximizes the deflection and stresses that are experienced by the tower. This ensures for the development of a conservative design for the material layout created through the optimization process.

4.4 Constraints

A series of constraints were applied to the system to provide guidelines to the optimization procedure. The optimization procedure operates at static equilibrium, with a bounded design vector. A maximum volume fraction was applied in order to ensure that the optimization system would proceed in a way that would favor solutions with a low total volume. (Eq. (3.16c)) The tower compliance minimization problem was solved originally using a material usage constraint C=0.25, which represents 25% of the original volume of the structure. The problem was also solved at 37.5%, 50%, and 75% volume of material to analyze the progression of the optimized solutions.

A potential issue in the optimization process can occur if the system does not converge to a solution within the prescribed limit. If this occurs, the optimization system will run for a specified maximum number of iterations and stop.

4.4.1 Tower Deflection

The power that can be produced from the wind turbine is affected by the deflection of the top of the tower. To insure that the savings that are achieved by the reduction in the volume of solid material do to the optimization of tower, are not outweighed by the reduction in the amount of power the turbine creates, the maximum deflection at the tower top is limited to 1.25% of the tower height. This limit

4.5 Penalization

The structural system is solved using a powerlaw mixing-rule, with a power (P), of 3.7. With a power greater than three, the system is highly penalized and is highly effective for the solution

for a structure consisting of solid/void material. The stiffness properties of the non-solid elements are reduced, which efficiently steer the solver away from partially solid structural elements and towards a solution that solely consists of solid or void elements.

CHAPTER 5. OPTIMIZATION RESULTS

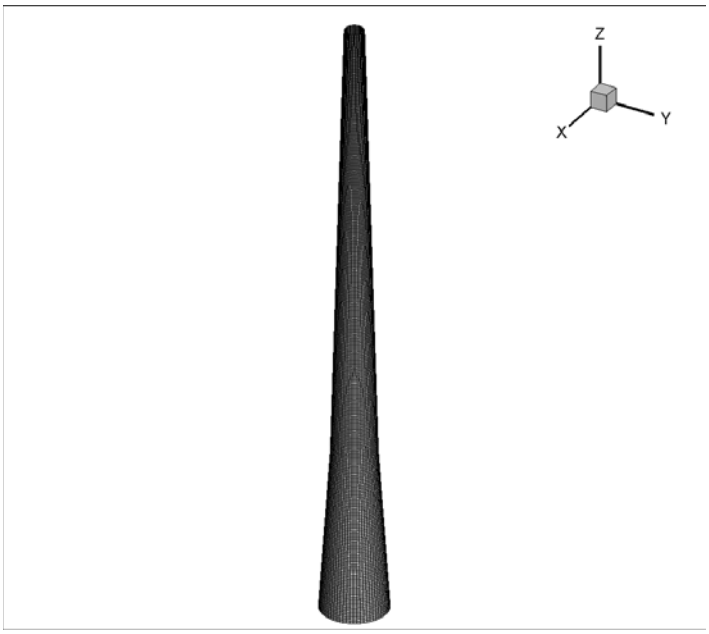

Figure 5-1: Tower model and mesh

The initial tower design space was a solid shell two taper tower with the dimensions shown in Tables 2-1, 2-2. To realistically model the necessary structure to support the design static wind load, as well as the gravity loads of the turbine components, topology optimization was performed to determine the layout that most efficiently uses the structural material.

The loading was applied to the structure as a system of effective forces to the nodes that comprise the top ring of the tower. Limiting the loading to those nodal points allowed the remaining nodes to be free to change their solid-void relationship according to the structural conditions, and not due to artificial constraints. The applied nodal forces are displayed in Table A-1.

The optimized tower under the specified loading conditions, resulted in the material layout shown in Figure 5-2. The optimized system is shown in enhanced detail in Figures 5-3 to 5-5.

Performing topology optimization on the statically loaded tower model resulted in the creation of a system that resembles that of an open lattice structure.

Figure 5-2: Optimized material layout

The top ring of the tower is completely solid which allows for it to support all the loading that is transferred from the nacelle to the tower. The top ring is supported a system of elements with a structure similar to a honeycomb consisting of diamond-shaped elements. This section is connected to the four steel columns that span a large section of the remaining tower.

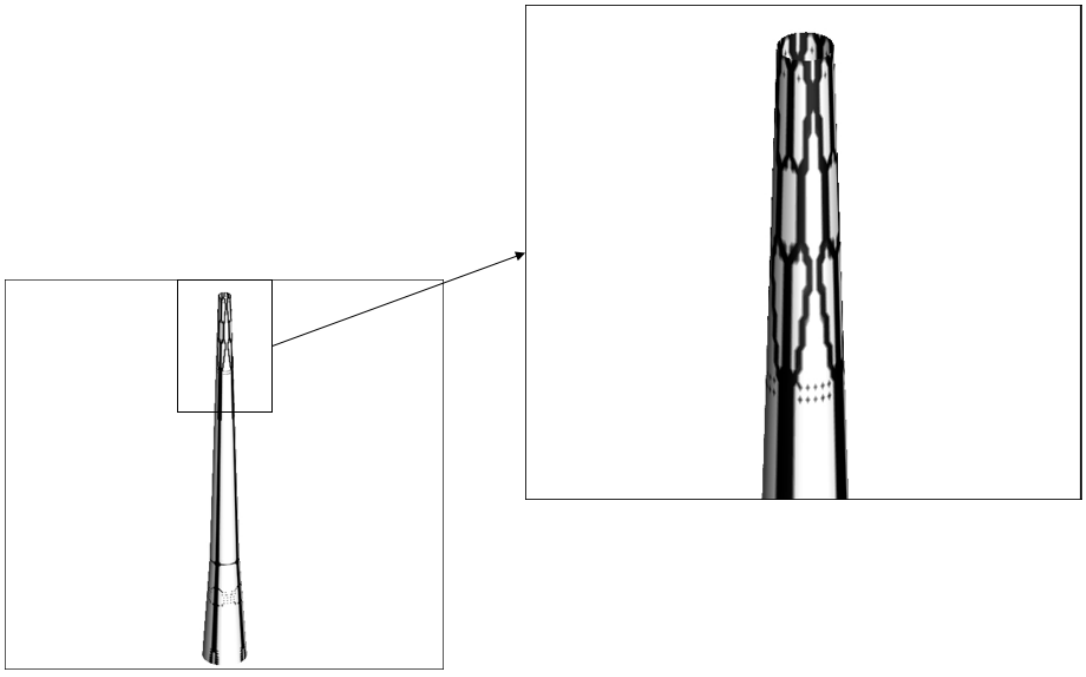

Figure 5-3: Optimized material layout (top)

The base of the tower consists of four small triangular elements, which support the four main structural columns. These columns have sections of lateral bracing, as well as cross bracing to provide lateral stability.

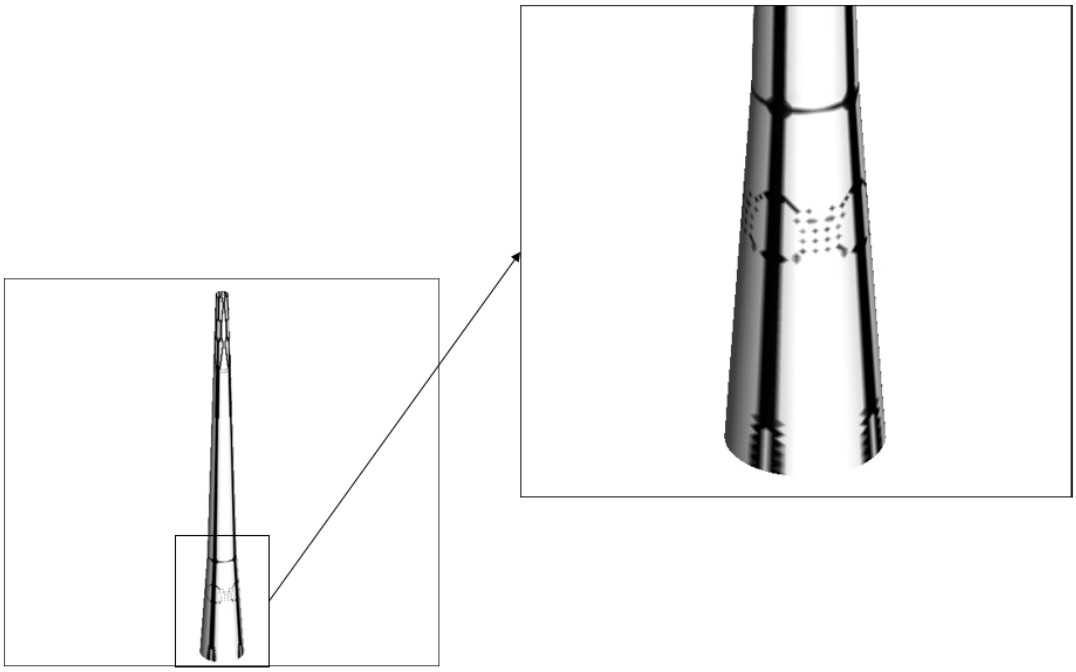

Figure 5-4: Optimized material layout (base)

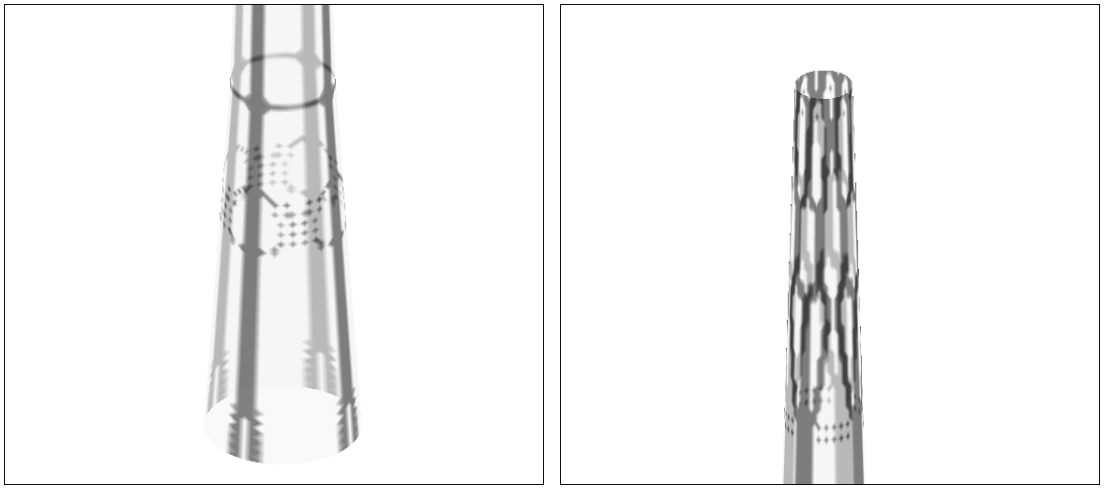

Figure 5-5: Transparent tower material layout

The optimized tower results in a final volume of 688m^2 of structural steel. However the tower experiences a maximum deflection that is greater than the maximum allowable, to avoid a reduction in power production.

Table 5-1: Results of optimization

Volume of Solid Material	688.22 m^3
Compliance of Structure	1.35E+10 kN*m
Maximum Deflection	2.8 m
Maximum Deflection as a Percentage of Tower Height	2.05 %

The material layout shows the most efficient positioning of the structural members. The model uses generic material properties and shapes, to create an image of the desired material layout. This would need to be recreated using sized structural members, to be analyzed for feasibility, in order to create a design that can be constructed. The optimization process is the first step in a multi-step procedure, aimed to provide insight into the ideal shape the system should take.

The deformed model show that the majority of the deflection occurs at the top half of the tower. Under design wind loading criteria the distortion of the tower occurs in the direction the force of the wind acts.

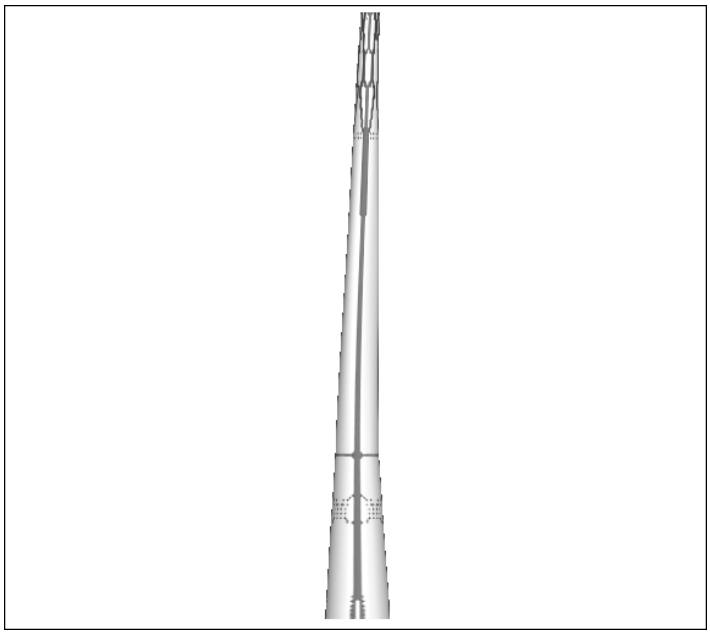

Figure 5-6: Deformed tower with optimized material layout

The tower optimization performed using the FENDAC and SLP programs was able to reach the desired volume fraction of 0.25, however the defection of that was experienced by the tower was more than the maximum allowable. This shows that the tower would not have the stiffness required to support the turbine with a 75% reduction in material from the original design.

To explore the progression of the optimum solutions of the tower problem, and find the percent of the original volume that could support the system, the test was run at four different material constraints. The problem was run for 75%, 50%, 37.5% in addition to the 25% material volume limit, and plotted to show the changes in the material layout of the structure.

The material is first removed from the lower portion of the tower. The tower has a double taper, and the bottom section has the largest cross sectional diameter and therefore moment of inertia. The material is removal gradually working its way up the tower. At 75% solid material triangular and diamond shaped void spaces are created in the lower portion of the tower shell.

When the amount of material is reduced to 50% of the original volume, the void spaces work their way further up the tower. The layout of solid material starts to form into four columns with lateral cross bracing. At both 37.5% and 25% of the original volume of material, the structure continues the progression to a solution of four columns. The structure gradually reduces the amount of material included in the structural columns, and cross bracing.

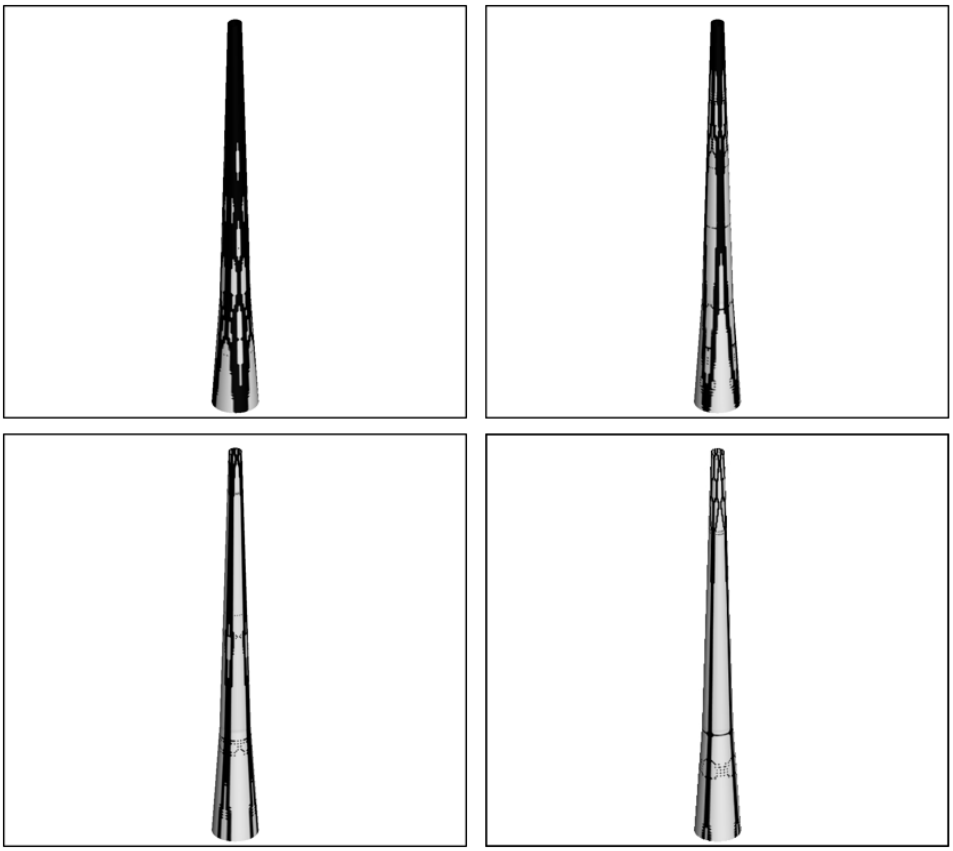

Figure 5-7: Optimal material layouts: 75% material (top-left), 50% material (top-right), 37.5% material (bottom-left), and 25% material (bottom-right)

The compliance of the structure follows an exponential trend in relation to the volume fraction of solid material in the system. The volume fraction of the ideal material layout for the turbine tower can be estimated for specified deflections using the trend data. Using the solutions of the optimization problems for the different volume fractions, the minimum percentage of the original volume which can meet the maximum deflection of 1.25%, is approximately 35% or roughly 1000m^2 of structural steel.

Table 5-2: Results of optimization at different volume fractions

Volume Percentage	Compliance (MN*m)	Deflection (Δ_{max}/height)
100%	1.52	--
75.0%	2.07	0.44%
50.0%	3.47	0.79%
37.5%	4.81	1.12%
25.0%	8.30	2.05%

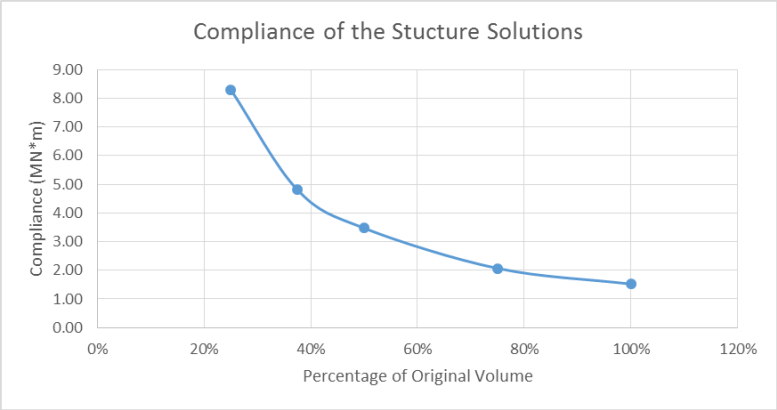

Figure 5-8: Compliance of the structure at different volume fractions

The structural model of the optimized tower could be brought to meet the maximum deflection limit by solving the optimization problem at a volume constraint of more than 35%. The material layout is solved for a constant shell thickness of 20cm. Therefore by creating a finite element model that follows the same pattern of as the optimal material layout, the model could be tested with different size and shape steel members to determine the tower structure that can support the loading, under the design criteria. By changing the size and shape of the members a structural stiffness of the tower can be manipulated to meet the desired criteria.

CHAPTER 6. SUMMARY

6.1 Conclusion

This study on the effectiveness of topology optimization of large utility wind turbines attempted to reduce the volume of the tower structure in an effort to reduce cost. The results showed that opening void spaces in the shell of the tower and creating an open lattice shape may be an effective method to reduce the volume of the structure, and potentially reduce the cost of construction. By reducing the cost to produce and erect the towers, it would make it more cost effective to use wind energy to create electricity and aid in the transition from fossil fuels to renewable energy sources.

The structure was able to meet all of the design criteria after undergoing a significant reduction in volume of solid material. The true deflection of the tower could be less then estimated, because of additional stiffening support from the elevator shaft, as well as a reduction of wind loading on the tower as a result of opening "holes" in the structure.

Calculations on the cost of the to construct the tower, (Table 6-1) shows that the capital cost of the tower could be significantly less than is estimated for the tower of the Enercon E-126. The cost calulations use a price of raw steel of $100 per ton, and that cost of raw materials make up 35% of the total construction cost, which falls with the 30%-40% range that is typical of steel construction projects.

Table 6-1: Estimated capital cost

Volume of Steel	688 m^3
Mass of Steel	5435.2 ton
Estimated Cost of Raw Material	$ 543,520.00
Estimated Cost of Tower	$ 1,550,000.00
Estimated Actual Cost of Tower	$ 3,700,000.00

6.2 Future Study

The results of the optimization procedure showed a large reduction in volume of the tower, from the initial design. The optimization process created a tower system which provided an open lattice steel structure which could support the static loading that would be experienced by the

tower under design wind loading. The next step would be to implement buckling and perimeter control constraints on the system. Employing these controls into the system would produce structure that is more conducive to conditions it would experience in the real world, and would be mesh independent.

There are different ways that the research could proceed after this step. The topology optimization problem could be solved for dynamic loading that the tower would experience under the conditions portrayed in IEC international standard for wind turbine design. Or size optimization could be performed on a representative beam element system, to determine the size of the members that would be need to support the loading with the material layout solution provided by the topology optimization problem. These steps would provide more results for more realistic conditions, and in turn allow for a more comprehensive analysis about the material efficiency of open lattice structures when compared to solid shell towers.

If the further studies show that the tower is competitive to that of the current towers, the last step would to be to create a structural finite element design for the tower, based on the optimization results, and preform a structural and cost analysis. This step would provide the evidence that steel truss based towers are, or are not more practical than reinforced concrete towers.

APPENDIX

Table A-1: Applied loading

Nodes	Fx (MN)	Fy (MN)	Fz (MN)	Nodes	Fx (MN)	Fy (MN)	Fz (MN)
17281	0.0507	0	-3.14	17313	0.0507	0	2.79
17282	0.0507	0	-3.12	17314	0.0507	0	2.78
17283	0.0507	0	-3.08	17315	0.0507	0	2.74
17284	0.0507	0	-3.00	17316	0.0507	0	2.67
17285	0.0507	0	-2.90	17317	0.0507	0	2.58
17286	0.0507	0	-2.77	17318	0.0507	0	2.46
17287	0.0507	0	-2.61	17319	0.0507	0	2.32
17288	0.0507	0	-2.43	17320	0.0507	0	2.16
17289	0.0507	0	-2.22	17321	0.0507	0	1.98
17290	0.0507	0	-1.99	17322	0.0507	0	1.77
17291	0.0507	0	-1.74	17323	0.0507	0	1.55
17292	0.0507	0	-1.48	17324	0.0507	0	1.32
17293	0.0507	0	-1.20	17325	0.0507	0	1.07
17294	0.0507	0	-0.91	17326	0.0507	0	0.81
17295	0.0507	0	-0.61	17327	0.0507	0	0.55
17296	0.0507	0	-0.31	17328	0.0507	0	0.27
17297	0.0507	0	0.00	17329	0.0507	0	0.00
17298	0.0507	0	0.27	17330	0.0507	0	-0.31
17299	0.0507	0	0.55	17331	0.0507	0	-0.61
17300	0.0507	0	0.81	17332	0.0507	0	-0.91
17301	0.0507	0	1.07	17333	0.0507	0	-1.20
17302	0.0507	0	1.32	17334	0.0507	0	-1.48
17303	0.0507	0	1.55	17335	0.0507	0	-1.74
17304	0.0507	0	1.77	17336	0.0507	0	-1.99
17305	0.0507	0	1.98	17337	0.0507	0	-2.22
17306	0.0507	0	2.16	17338	0.0507	0	-2.43
17307	0.0507	0	2.32	17339	0.0507	0	-2.61
17308	0.0507	0	2.46	17340	0.0507	0	-2.77
17309	0.0507	0	2.58	17341	0.0507	0	-2.90
17310	0.0507	0	2.67	17342	0.0507	0	-3.00
17311	0.0507	0	2.74	17343	0.0507	0	-3.08
17312	0.0507	0	2.78	17344	0.0507	0	-3.12

Table A-2: Pressure coefficients (C_q) Uniform Building Code 1997

STRUCTURE OR PART THEREOF	DESCRIPTION	C_q FACTOR
1. Primary frames and systems	**Method 1** (Normal force method)	
	Walls:	
	Windward wall	0.8 inward
	Leeward wall	0.5 outward
	Roofs[1]:	
	Wind perpendicular to ridge	
	Leeward roof or flat roof	0.7 outward
	Windward roof	
	less than 2:12 (16.7%)	0.7 outward
	Slope 2:12 (16.7%) to less than 9:12 (75%)	0.9 outward or 0.3 inward
	Slope 9:12 (75%) to 12:12 (100%)	0.4 inward
	Slope > 12:12 (100%)	0.7 inward
	Wind parallel to ridge and flat roofs	0.7 outward
	Method 2 (Projected area method)	
	On vertical projected area	
	Structures 40 feet (12 192 mm) or less in height	1.3 horizontal any direction
	Structures over 40 feet (12 192 mm) in height	1.4 horizontal any direction
	On horizontal projected area[1]	0.7 upward
2. Elements and components not in areas of discontinuity[2]	Wall elements	
	All structures	1.2 inward
	Enclosed and unenclosed structures	1.2 outward
	Partially enclosed structures	1.6 outward
	Parapets walls	1.3 inward or outward
	Roof elements[3]	
	Enclosed and unenclosed structures	
	Slope < 7:12 (58.3%)	1.3 outward
	Slope 7:12 (58.3%) to 12:12 (100%)	1.3 outward or inward
	Partially enclosed structures	
	Slope < 2:12 (16.7%)	1.7 outward
	Slope 2:12 (16.7%) to 7:12 (58.3%)	1.6 outward or 0.8 inward
	Slope > 7:12 (58.3%) to 12:12 (100%)	1.7 outward or inward
3. Elements and components in areas of discontinuities[2,4,5]	Wall corners[6]	1.5 outward or 1.2 inward
	Roof eaves, rakes or ridges without overhangs[6]	
	Slope < 2:12 (16.7%)	2.3 upward
	Slope 2:12 (16.7%) to 7:12 (58.3%)	2.6 outward
	Slope > 7:12 (58.3%) to 12:12 (100%)	1.6 outward
	For slopes less than 2:12 (16.7%)	
	Overhangs at roof eaves, rakes or ridges, and canopies	0.5 added to values above
4. Chimneys, tanks and solid towers	Square or rectangular	1.4 any direction
	Hexagonal or octagonal	1.1 any direction
	Round or elliptical	0.8 any direction
5. Open-frame towers[7,8]	Square and rectangular	
	Diagonal	4.0
	Normal	3.6
	Triangular	3.2
6. Tower accessories (such as ladders, conduit, lights and elevators)	Cylindrical members	
	2 inches (51 mm) or less in diameter	1.0
	Over 2 inches (51 mm) in diameter	0.8
	Flat or angular members	1.3
7. Signs, flagpoles, lightpoles, minor structures[8]		1.4 any direction

[1]For one story or the top story of multistory partially enclosed structures, an additional value of 0.5 shall be added to the outward C_q. The most critical combination shall be used for design. For definition of partially enclosed structures, see Section 1616.

[2]C_q values listed are for 10-square-foot (0.93 m^2) tributary areas. For tributary areas of 100 square feet (9.29 m^2), the value of 0.3 may be subtracted from C_q, except for areas at discontinuities with slopes less than 7 units vertical in 12 units horizontal (58.3% slope) where the value of 0.8 may be subtracted from C_q. Interpolation may be used for tributary areas between 10 and 100 square feet (0.93 m^2 and 9.29 m^2). For tributary areas greater than 1,000 square feet (92.9 m^2), use primary frame values.

[3]For slopes greater than 12 units vertical in 12 units horizontal (100% slope), use wall element values.

[4]Local pressures shall apply over a distance from the discontinuity of 10 feet (3048 mm) or 0.1 times the least width of the structure, whichever is smaller.

[5]Discontinuities at wall corners or roof ridges are defined as discontinuous breaks in the surface where the included interior angle measures 170 degrees or less.

[6]Load is to be applied on either side of discontinuity but not simultaneously on both sides.

[7]Wind pressures shall be applied to the total normal projected area of all elements on one face. The forces shall be assumed to act parallel to the wind direction.

[8]Factors for cylindrical elements are two thirds of those for flat or angular elements.

Table A-3: Wind load at specified tower height

Height (m)	Wind Force (kN)	Height (m)	Wind Force (kN)
0	0	66	141.97
1	43.8	67	141.91
2	56.57	68	141.82
3	65.98	69	141.72
4	73.59	70	141.6
5	80.02	71	141.45
6	85.59	72	141.29
7	90.5	73	141.11
8	94.86	74	140.91
9	98.79	75	140.69
10	102.33	76	140.45
11	105.55	77	140.19
12	108.47	78	139.92
13	111.14	79	139.63
14	113.57	80	139.32
15	115.79	81	138.99
16	117.82	82	138.65
17	119.67	83	138.28
18	121.36	84	137.91
19	122.89	85	137.51
20	124.28	86	137.11
21	125.53	87	136.68
22	126.66	88	136.24
23	127.67	89	135.78
24	128.56	90	135.31
25	129.34	91	134.82
26	130.02	92	134.32
27	130.61	93	133.8
28	131.1	94	133.27
29	131.49	95	132.73
30	131.81	96	132.16
31	132.03	97	131.59
32	132.18	98	131
33	132.25	99	130.4
34	132.25	100	129.78
35	132.17	101	129.15
36	132.02	102	128.51
37	131.81	103	127.85
38	133.35	104	127.18

Table A-3—continued

39	134.09	105	126.5
40	134.78	106	125.8
41	135.44	107	125.09
42	136.05	108	124.37
43	136.64	109	123.63
44	137.19	110	122.88
45	137.7	111	122.12
46	138.18	112	121.35
47	138.63	113	120.57
48	139.05	114	119.77
49	139.44	115	118.96
50	139.8	116	118.14
51	140.13	117	117.31
52	140.43	118	116.47
53	140.7	119	115.61
54	140.95	120	114.74
55	141.17	121	113.86
56	141.36	122	112.97
57	141.53	123	112.07
58	141.67	124	111.16
59	141.79	125	110.24
60	141.88	126	109.3
61	141.95	127	108.36
62	142	128	107.4
63	142.03	129	106.44
64	142.03	130	105.46
65	142.01	Total Force	16425.57

Table A-4: Calculated loading on nodes due to turbine components

Nodes	Gravity Load (MN)	Resultant Bending Moment (MN)	Total Force (MN)	Effective Point Load (MN)
17281	-28.4	-6.25	-34.66	-4.22
17282	-28.13	-6.2	-34.33	-4.18
17283	-27.86	-6.14	-34	-4.14
17284	-27.06	-5.97	-33.03	-4.03
17285	-26.26	-5.8	-32.06	-3.91
17286	-24.96	-5.52	-30.48	-3.71
17287	-23.66	-5.24	-28.9	-3.52
17288	-21.91	-4.87	-26.78	-3.26
17289	-20.16	-4.5	-24.66	-3.01
17290	-18.03	-4.04	-22.07	-2.69
17291	-15.9	-3.59	-19.48	-2.37
17292	-13.46	-3.07	-16.53	-2.01
17293	-11.03	-2.55	-13.58	-1.66
17294	-8.39	-1.99	-10.38	-1.26
17295	-5.75	-1.43	-7.18	-0.87
17296	-3	-0.84	-3.85	-0.47
17297	-0.26	-0.26	-0.52	-0.06
17298	2.49	0.33	2.81	0.34
17299	5.23	0.91	6.14	0.75
17300	7.87	1.47	9.35	1.14
17301	10.51	2.04	12.55	1.53
17302	12.95	2.55	15.5	1.89
17303	15.38	3.07	18.45	2.25
17304	17.51	3.53	21.04	2.56
17305	19.64	3.98	23.63	2.88
17306	21.39	4.35	25.75	3.14
17307	23.14	4.73	27.87	3.4
17308	24.45	5	29.45	3.59
17309	25.75	5.28	31.03	3.78
17310	26.55	5.45	32	3.9
17311	27.35	5.62	32.97	4.02
17312	27.62	5.68	33.3	4.06
17313	27.89	5.74	33.63	4.1
17314	27.62	5.68	33.3	4.06
17315	27.35	5.62	32.97	4.02
17316	26.55	5.45	32	3.9
17317	25.75	5.28	31.03	3.78
17318	24.45	5	29.45	3.59

Table A-4—continued

17319	23.15	4.73	27.87	3.4
17320	21.4	4.35	25.75	3.14
17321	19.65	3.98	23.63	2.88
17322	17.51	3.53	21.04	2.56
17323	15.38	3.07	18.46	2.25
17324	12.95	2.55	15.5	1.89
17325	10.52	2.04	12.55	1.53
17326	7.88	1.47	9.35	1.14
17327	5.24	0.91	6.15	0.75
17328	2.49	0.33	2.82	0.34
17329	-0.25	-0.26	-0.51	-0.06
17330	-3	-0.84	-3.84	-0.47
17331	-5.75	-1.43	-7.17	-0.87
17332	-8.39	-1.99	-10.38	-1.26
17333	-11.03	-2.55	-13.58	-1.65
17334	-13.46	-3.07	-16.53	-2.01
17335	-15.89	-3.59	-19.48	-2.37
17336	-18.03	-4.04	-22.07	-2.69
17337	-20.16	-4.5	-24.65	-3
17338	-21.91	-4.87	-26.78	-3.26
17339	-23.66	-5.24	-28.9	-3.52
17340	-24.96	-5.52	-30.48	-3.71
17341	-26.26	-5.8	-32.06	-3.91
17342	-27.06	-5.97	-33.03	-4.03
17343	-27.86	-6.14	-34	-4.14
17344	-28.13	-6.2	-34.33	-4.18

REFERENCES

[1] Al Rabadi, Haitham Farah Hanna. "Truss size and topology optimization using harmony search method." MS (Master of Science) thesis, University of Iowa, 2014.http://ir.uiowa.edu/etd/1424.

[2] Arora, J.S. Introduction to optimum design. New York. McGraw-Hill, 2012. ISBN 007002460X

[3] Beghini, L. L. “Building science through topology optimization” (Doctoral dissertation). University of Illinois at Urbana-Champaign, 2013.

[4] Bendsoe, M. P. and O Sigmund. *Topology Optimization: Theory, Methods and Applications*. Springer, 2002.

[5] Bir, Gunjit S., and J. M. Jonkman. *Modal Dynamics of Large Wind Turbines with Different Support Structures*. Golden, Colo.: National Renewable Energy Laboratory, 2008.

[6] Bradley, Dave. "WAG - Wind Action Group Engineering: The Big News and Hidden News." *WAG - Wind Action Group Engineering: The Big News and Hidden News*. Web. 19 Oct. 2014. <http://wagengineering.blogspot.com/2012/05/big-news-and-hidden-news.html>.

[7] Burton, T., Sharpe, D., Jenkins, N., & Bossanyi, E. 2001. *Wind Energy Handbook.* West Sussex, England: John Wiley & Sons Ltd.

[8] Catalano, Pietro, Meng Wang, Gianluca Iaccarino, and Parviz Moin. "Numerical Simulation of the Flow around a Circular Cylinder at High Reynolds Numbers." *International Journal of Heat and Fluid Flow*: 463-69.

[9] Connell JR. The spectrum of wind speed fluctuations encountered by a rotating blade of a wind energy conversion system. Solar Energy 1982;29(5):363–75.

[10] "CONSTRUCTION." - *Wind Systems Magazine*. Web. <http://www.windsystemsmag.com/article/detail/102/construction>.

[11] De Vries, Eize. "E-126 in Action: Enercon's Next-Generation Power Plant." *RenewableEnergy World*. 16 Sept. 2009. Web. 8 Oct. 2014. <http://www.renewableenergyworld.com/rea/news/article/2009/09/e-126-in-action-enercons-next-generation-power-plant>.

[12] "Enercon E-126." - *The Largest Wind Turbine*. Web. 2 Oct. 2014. <http://www.solarenergytopics.com/wind/enercon-e126-largest-wind-turbine.html>.

[13] "Enercon E126/6000." *Enercon E126/6000*. Web. <http://www.thewindpower.net/turbine_en_223_enercon_e126-6000.php>.

[14] "Energy: What Do We Want to Achieve? - European Commission." *Energy: What Do We Want to Achieve? - European Commission*. Web. 29 Oct. 2014. <http://ec.europa.eu/energy/renewables/index_en.htm>.

[15] "Exposure Categories." *Exposure Categories*. Web. 13 Oct. 2014. <http://www.worldtower.com/QR_222_G_Exp.htm>.

[16] Fool, Matt DiLallo The Motley. "The World Has 53.3 Years of Oil Left." *USA Today*. Gannett, 28 June 2014. Web. 03 July 2015. <http://www.usatoday.com/story/money/business/2014/06/28/the-world-was-533-years-of-oil-left/11528999/>.

[17] "Foundations." *Wind Farms Construction*. Web. <http://www.windfarmbop.com/category/foundations/page/2/>.

[18] Ghedin, Federico. " Structural Design of a 5 MW Wind Turbine Blade Equipped with Boundary Layer Suction Technology." MS (Master of Science) thesis, Eindhoven University of Technology, 2010.

[19] "Global Statistics." *GWEC*. Web. 25 Mar. 2015.Hau E. Wind turbines: fundamentals, technologies, applications, economics. 2nd ed. Berlin: Springer; 2006.

[20] Grünberg, Jürgen, Joachim Göhlmann, and Philip Thrift. *Concrete Structures for Wind Turbines*. Print

[21] Harte R, Van Zijl GPAG. Structural stability of concrete wind turbines and solar chimney towers exposed to dynamic wind action. J Wind Eng Ind Aerodyn 2007;95(9–11):1079–96.

[22] Hillmer, B., T. Borstelmann, P A Schaffarczyk, and L. Dannenberg. "Aerodynamic and Structural Design of MultiMW Wind Turbine Blades beyond 5MW." *Journal of Physics: Conference Series* (2007).

[23] Hughes, T.J.R. “The Finite Element Method: Linear Static and Dynamic Finite Element Analysis”, Prentice-Hall, 1987.

[24] Ingram, Grant. "Wind Turbine Blade Analysis using the Blade Element Momentum Method. Version 1.0." *School of Engineering, Durham University, UK* (2005).

[25] International Electrotechnical Commission (IEC). 2005. *Wind Turbines – Part 1:Design Requirements* (61400-1). Geneva, Switzerland: International Electrotechnical Commission (IEC).

[26] Jonkman, J. M. *Definition of a 5-MW Reference Wind Turbine for Offshore System Development*. Golden, Colo.: National Renewable Energy Laboratory, 2009.

[27] Kocer, Fatma Y. and Arora, Jasbir S. 1996. Design of Prestressed Concrete Transmission Poles: Optimization Approach. *Journal of Structural Engineering* 122,no. 7 (July): 804-814.

[28] Kocer, Fatma Y. and Arora, Jasbir S. 1996. Optimal Design of Steel Transmission Poles. *Journal of Structural Engineering* 122, no. 11 (November): 1347-1356.

[29] Lakehal, D. "Computation of Turbulent Shear Flows over Rough-walled Circular Cylinders." *Journal of Wind Engineering and Industrial Aerodynamics*: 47-68.

[30] Lavassas, I., G. Nikolaidis, P. Zervas, E. Efthimiou, I.n. Doudoumis, and C.c. Baniotopoulos. "Analysis and Design of the Prototype of a Steel 1-MW Wind Turbine Tower." *Engineering Structures* (2003): 1097-106.

[31] Linero, D. L., Oliver, X., Huespe, A. E., A model of material failure for reinforced concrete via continuum strong discontinuity approach and mixing theory. Barcelona, International Center for Numerical Methods in Engineering, 2007.

[32] Lu, Bodi. "Conceptual design using multilevel continuum structural topology optimization." MS (Master of Science) thesis, University of Iowa, 2014. http://ir.uiowa.edu/etd/4685.

[33] Man, X. "A Mathematical and Computational Multiscale Clothing Modeling Framework", PhD Dissertation, The University of Iowa, (2006)

[34] Mijar, A. R. (1997). Topology design of structures using SLP. (Master thesis). University of Iowa.

[35] "Montage Von Zwei Enercon E 126 Windenergieanlagen - Hansebube.de." *Montage Von Zwei Enercon E 126 Windenergieanlagen - Hansebube.de*. Web. <http://www.hansebube.de/eins/altenwerder/bild66.html>.

[36] Negm, Hani M. and Maalawi, Karam Y. 1999. Structural Design Optimization of Wind Turbine Towers. *Computers and Structures* 74 (2000): 649-666.

[37] "Newton's Nose-Cone Problem." *D:MyDocswebarticlesnoseconenosecone.htm*. Web. 25 Oct. 2014. <http://wps.prenhall.com/wps/media/objects/4559/4668829/chapt4/ proj4.3C/ nosecone/nosecone.htm>.

[38] Nicholson, John Corbett. "Design of wind turbine tower and foundation systems: optimization approach." MS (Master of Science) thesis, University of Iowa, 2011. http://ir.uiowa.edu/etd/1042.

[39] "Offshore Wind Turbines Transporters Rise to the Challenge. Part 1." *Offshore Wind Turbines Transporters Rise to the Challenge. Part 1*. Web. <http://www.radiolocman.com/review/article.html?di=125795>.

[40] Ohsaki, M., & Swan, C. C. (2002). Topology and geometry optimization of trusses and frames. Recent Advances in Optimal Structural Design, 97-123.

[41] Parish, Scott. *Uniform Building Code Compliance Manual: 1997 Uniform Building Code*. New York: McGraw-Hill, 1999.

[42] Paulman, Ken. "Breaking down the Costs of Wind Turbine Components." *Midwest Energy News*. N.p., 27 Mar. 2012. Web. 25 Mar. 2015.

[43] "PILE FOUNDATION - NEED AND FUNCTIONS." *The Constructor*. 17 Nov. 2014. Web. <http://theconstructor.org/geotechnical/foundations/need-functions-of-pile-foundation/1785/>.

[44] "Project." *Solaripedia*. Web. <http://www.solaripedia.com/13/201/2018/enercon_e126_nose_interior.html>.

[45] Pyper, Julia. "European Union Sets Ambitious 2030 Climate and Energy Goals : Greentech Media." *European Union Sets Ambitious 2030 Climate and Energy Goals : Greentech Media*. Web. 29 Oct. 2014. <http://www.greentechmedia.com/articles/read/european-union-sets-ambitious-2030-climate-and-energy-goals>.

[46] Quilligan, A., A. O'Connor, and V. Pakrashi. "Fragility Analysis of Steel and Concrete Wind Turbine Towers." *Engineering Structures* (2012): 270-82.

[47] "RENEWABLE ENERGY TECHNOLOGIES: COST ANALYSIS SERIES." *IRENA WORKING PAPER* Volume 1: Power Sector.5 (2012). <www.irena.org/Publications>.

[48] Reddy, B. Siva Konda, V.Rohini Padmavathi, and Ch. Srikanth. "STUDY OF WIND LOAD EFFECTS ON TALL RC CHIMNEYS." *International Journal of Advanced Engineering Technology* III.II (2012).

[49] "Renewable Energy Standards." *SEIA*. Web. 29 Oct. 2014. <http://www.seia.org/policy/renewable-energy-deployment/renewable-energy-standards>.

[50] Resor, Brian. "Definition of a 5MW/61.5m Wind Turbine Blade Reference Model." *SANDIA REPORT* (2013).

[51] Riso and DNV. 2002. *Guidelines for Design of Wind Turbines*. http://www.risoe.dk/en/business_relations/Products_Services/consultancy_service/VEA_guidelines/~/media/Risoe_dk/Erhvervskontakt/VEA/Documents/All_corrections.ashx

[52] R.Merrick and G.Bitsuamlak, "Control of flow around a circular cylinder by the use of surface roughness: A computational and experimental approach".

[53] Rooij, R. v., Terminology, Reference Systems and Conventions, Delft: R. van Rooij, 2001.

[54] Schwabe, Paul, Sander Lensink, and M. Maureen. Hand. *IEA Wind Task 26. Multi-national Case Study of the Financial Cost of Wind Energy*. Golden, CO: National Renewable Energy Laboratory, 2010. Web.

[55] Schweilger, Katharina Mairead. " Aerodynamic Analysis of the NREL 5-MW Wind Turbine using Vortex Panel Method." MS (Master of Science) thesis, Chalmers University of Technology, 2012.

[56] Simiu E, Scanlan RH. Wind effects on structures: fundamentals and applications to design. 3rd ed. New York: John Wiley & Sons; 1996.

[57] Singh, A.N. "Concrete Construction for Wind Energy Towers." *The Indian Concrete Journal* (2007): 43-49.

[58] "Solar #2 New Energy Source In 2013 (US)." *CleanTechnica*. Web. 3 Oct. 2014. <http://cleantechnica.com/2014/01/28/solar-surpasses-natural-gas-part-us-energy-infrastructure/>.

[59] Sorensen JD, Toft HS. Probabilistic design of wind turbines. Energies 2010; 3:241–57.

[60] C.C. Swan and J.S. Arora, "Topology design of material layout in structured composites of high stiffness and strength," Structural Optimization **13**(1) 45-59 (1997).

[61] Swan, C. C., Topology optimization with engineering application. Unpublished. (2013).

[62] Swan, C. C., Kosaka, I. Voigt-Reuss topology optimization for structures with nonlinear material behaviors. International Journal for Numerical Methods in Engineering, Vol. 40, 3785-3814 (1997).

[63] Symons, Digby. "Mechanical Engineering for Renewable Energy Systems." *ENGINEERING TRIPOS PART IB PAPER 8 – ELECTIVE (2)* (2009). Web. <http://www2.eng.cam.ac.uk/~hemh/climate/P8_Blade_Design_ Student_Handout_2009. pdf>.

[64] "Twinkle Toes Engineering." *Twinkle Toes Engineering*. Web. 5 Nov. 2014. <http://twinkle_toes_engineering.home.comcast.net/~twinkle_toes_engineering/wind_turbine.html>.

[65] Umut, Önder, Bülent Akbas, and Jay Shen. "Design Issues of Wind Turbine Towers." *Proceedings of the 8th International Conference on Structural Dynamics* (2011).

[66] "U.S. Energy Information Administration - EIA - Independent Statistics and Analysis." *How Much of World Energy Consumption and Electricity Generation Is from Renewable Energy* Web.

[67] Vesel Jr., Richard W. " Aero-Structural Optimization of a 5 MW Wind Turbine Rotor." MS (Master of Science) thesis, The Ohio State University, 2012.

[68] Wang, Meng, Catalano Catalano, and Gianluca Iaccarino. "Prediction of High Reynolds Number Flow over a Circular Cylinder Using LES with Wall Modeling." *Center for Turbulence Research* Annual Research Briefs (2001): 45-50.

[69] Wind Energy Facts at a Glance." *Wind Energy Facts at a Glance*. American Wind Energy Association, Web.

[70] "Wind Energy Pros and Cons - Energy Informative." *Energy Informative*. Web. 29 Sept. 2014. <http://energyinformative.org/wind-energy-pros-and-cons/>.

[71] Wind turbines-part 1: design requirements. British Standards Institution; 2005.

[72] "World’s Most Powerful Wind Turbine May Undergo High Winds Tests." *CleanTechnica*. Web. 2 Oct. 2014. <http://cleantechnica.com/2013/08/23/worlds-most-powerful-wind-turbine-may-undergo-high-winds-coastal-tests/>.

[73] Zipp, Kathleen. "Understanding Costs for Large Wind-turbine Drivetrains." *Windpower Engineering Development*. Web.